# Identification of complex non-linear modes of mechanical systems using the Hilbert-Huang transform from free decay responses

V. Ondra[a,*], I.A. Sever[b], C.W. Schwingshackl[c]

[a] *Rolls-Royce plc., BS34 7QE Bristol, United Kingdom*
[b] *Rolls-Royce plc., DE24 8BJ Derby, United Kingdom*
[c] *Imperial College London, Mechanical Engineering, Exhibition Road, SW7 2AZ London, United Kingdom*

**Abstract**

Modal analysis is a well-established method for analysis of linear systems, but its extension to non-linear structures has proven to be much more problematic. Several competitive definitions of non-linear modes and a variety of experimental methods have been introduced. In this paper, the definition of complex non-linear modes (CNMs) of mechanical systems is adopted and the possibility of their identification from experimental free decay responses using the Hilbert-Huang transform (HHT) is explored. It is firstly discussed that since there are similarities in the definition of intrinsic mode functions obtained using the HHT and reduced order model of slow-flow dynamics based on the CNMs, there is a reason to believe that the HHT can indeed extract the CNMs. This paper, however, presents a new insight into the use of the Hilbert-Huang transform by showing that the amplitude-dependent frequency and damping extracted from a free decay response are only suitable for detection and characterisation of non-linearities, but they cannot be used to quantify the non-linear behaviour by fitting the CNMs even if a model of the system is known. The analytical proof of the HHT cannot be currently formulated due to a limited understanding of its empirical nature. Instead, this unconventional conclusion is supported by a series of numerical studies of conservative and non-conservative non-linear systems with a wide range of parameters. In all cases, a special care is taken to apply the basic HHT only on such signals for which mode separation is possible (no mode-mixing occurs). This eliminates the need for more sophisticated HHT versions and clearly demonstrates the inability of the HHT to extract CNMs even for the simplest cases. In addition to numerical studies, the identification of several non-linear modes is demonstrated experimentally using the free decay responses obtained from the ECL benchmark. It is shown that the HHT is able to successfully extract several non-linear modes whose character correspond to the numerical reference, but which cannot be used to quantify the system parameters due to conclusions made in this paper. The findings highlight that the ability of the HHT to quantify non-linear behaviour using non-linear modes extracted from free decay responses is severely limited, while detection and characterisation of non-linear behaviour in a non-parametric manner is feasible.

*Keywords:* Hilbert-Huang transform, Complex non-linear modes, Reduced order model, Slow-flow dynamics, Non-linear system identification

## Highlights

- Identification of complex non-linear modes using the Hilbert-Huang transform (HHT) is presented
- The ability of the HHT to identify the complex non-linear modes is numerically investigated
- The findings highlight that the HHT can detect and characterise, but not quantify, non-linear behaviour

*Corresponding author.
*Email addresses:* vaclav.ondra@rolls-royce.com (V. Ondra), ibrahim.sever@rolls-royce.com (I.A. Sever), c.schwingshackl@imperial.ac.uk (C.W. Schwingshackl)

- The estimation of complex non-linear modes is also demonstrated experimentally

**Nomenclature**

| Symbol | Description |
|---|---|
| $a(t)$ | Instantaneous amplitude |
| $c_{\mathrm{nl}}$ | Non-linear damping coefficient |
| $c(t)$ | Intrinsic mode function |
| $C_m^{(k)}$ | Correlation coefficient for the $k$-th mass and $m$-th mode |
| $d(t)$ | Logarithm of the instantaneous amplitude |
| $e_{\min}$, $e_{\max}$ | Upper and lower envelope |
| $E$ | Young's modulus |
| $f(t)$ | Instantaneous frequency |
| $\mathbf{f}$ | Vector of non-linear forces |
| $h(t)$ | Proto-mode function |
| $k_{\mathrm{nl}}$ | Non-linear stiffness coefficient |
| $L$, $W$ | Length of a beam and width of its cross section |
| $m$, $c$, $k$ | Mass, damping and stiffness coefficient |
| $\mathbf{M}$, $\mathbf{C}$, $\mathbf{K}$ | Mass, damping and stiffness matrix |
| $N_{\mathrm{h}}$ | Number of harmonics |
| $N_{\mathrm{IMF}}$ | Number of intrinsic mode functions |
| $q$ | Modal amplitude |
| $r(t)$ | Residuum |
| $t$ | Time |
| $\mathbf{t}$ | Complex vector for phase normalisation |
| $x(t)$ | Displacement |
| $\mathbf{x}(t)$, $\dot{\mathbf{x}}(t)$, $\ddot{\mathbf{x}}(t)$ | Vectors of displacement, velocity and acceleration |
| $z(t)$ | Analytic signal |
| $\alpha$, $\beta$ | Coefficients of viscous proportional damping |
| $\delta$ | Damping rate |
| $\zeta$ | Damping ratio |
| $\theta(t)$ | Phase |
| $\Theta(t)$ | Slow phase |
| $\lambda$ | Complex fundamental eigenfrequency |
| $\boldsymbol{\nu}$ | Manifold |
| $\rho$ | Density |
| $\phi(t)$ | Fast phase |
| $\boldsymbol{\phi}$ | Estimated non-linear mode |
| $\boldsymbol{\Psi}$ | Complex eigenvector |
| $\omega$ | Angular frequency |
| $\Omega$ | Excitation frequency |
| pv | Cauchy principal value of the integral |
| $\langle\,,\,\rangle$ | Operator of generalised Fourier coefficients |
| $\tilde{\bullet}$ | Hilbert transform |
| AFT | Alternating frequency-time procedure |
| CNM | Complex non-linear mode |
| CxA | Complexification-averaging |
| ECL | École Centrale de Lyon |
| EEMD | Ensemble empirical mode decomposition |
| EMD | Empirical mode decomposition |
| FE | Finite element |

| | |
|---|---|
| FFT | Fast Fourier transform |
| FRF | Frequency response function |
| HHT | Hilbert-Huang transform |
| HHSA | Holo-Hilbert spectral analysis |
| HT | Hilbert transform |
| IA | Instantaneous amplitude |
| IF | Instantaneous frequency |
| IMF | Intrinsic mode function |
| MDOF | Multi-degree-of-freedom |
| NNM | Non-linear normal mode |
| ROM | Reduced order model of slow-flow dynamics based on CNMs |
| SDOF | Single-degree-of-freedom |
| WBEMD | Wavelet-bounded empirical mode decomposition |
| ZC | Zero-crossing |

## 1. Introduction

Modal analysis is a well-established method for the analysis of linear dynamic structures [1], but its extension to non-linear structures has proven to be much more problematic. Some might even question the philosophy of non-linear modal analysis as pointed out in [2, 3]. Nonetheless, a number of viewpoints on non-linear modal analysis exists, each of which tries to preserve a subset of properties of the original linear modal analysis. The non-linear modes have been actively studied for several decades so a range of methods for their numerical computation [4] as well as experimental investigation [5, 6] have been developed, and a number of reviews have been written [7–12].

Non-linear normal modes (NNMs) were originally defined as motions in unison of a conservative system [13]. Such definition requires all points of the system to reach their extreme values and pass through zero simultaneously. However, this definition could not capture modal interactions during which the periodic motion consists of at least two interacting modes of different frequencies, and the system can no longer vibrate in unison. To account for modal iterations, the original definition must have been later extended, defining an NNM as a non-necessarily synchronous periodic motion of a conservative mechanical system. This definition has been adopted in a number of studies [7, 14–17], partly because it enables an effective numerical computation of NNMs [4]. The NNMs can generally undergo bifurcations and stability changes, and experience internal resonances. However, they are not defined in the presence of damping (although the dynamics of lightly damped non-linear systems may be sometimes still interpreted using NNMs of underlying conservative systems [7]). At the same time, however, complex damping mechanisms can occur in engineering assemblies, for instance in form of joints and interfaces, and even linear viscous damping of components may sometimes significantly alter the dynamics of a structure. Therefore, an alternative definition of NNMs for damped systems was proposed in [18]. In this approach, an NNM is defined as a two-dimensional surface, termed invariant manifold, in the phase space. Trajectories of motions that started on this manifold remain on it for all time so the system effectively behaves as a non-linear SDOF system.

More recently, complex non-linear modes (CNMs) have been proposed in [19] and their use has been extended for non-linear modal synthesis, harmonically forced and self-excited systems in [20]. A complex non-linear mode of motion is defined as an oscillation of the autonomous system with (potentially) a phase difference between its degrees of freedom. The CNMs allow direct computation of amplitude-dependent frequency, damping and mode shape at the resonance in a timely-fashion. Moreover, the numerical implementation of the CNMs does not require significant modifications to conventional harmonic balance solvers. The ability of CNMs to deal with large non-conservative systems and general types of non-linearities led to their application to bladed disks coupled by mechanical joints with friction interfaces [19, 21, 22]. In [23], the CNMs were used for the derivation of reduced order models (ROM) of slow-flow dynamics of the system. The concepts of CNMs and ROM are adopted throughout this study.

There is a great number of methods for non-linear system identification available in literature. They can be divided into a number of groups as in [24], including time-domain (e.g. restoring force surface [25],

NARMAX [26]) and frequency-domain methods (e.g. Volterra series [2]), time-frequency analysis (e.g. Short-time Fourier transform [27], Wavelet transform [28]) and structural model updating. Each group of methods is suitable for a different application and provides different information. Some of them also require a special type of excitation. Therefore, not all of them can be used to identify the non-linear modes. Non-linear modes are often investigated using phase resonance testing (also known as force appropriation) [14, 15, 17, 29], which eliminates the need to decompose measured signals. However, multi-modal non-linear identification through the direct decomposition of experimental measurements by the Hilbert-Huang transform into a set of oscillatory functions has also been presented in a number of papers [30–35]. It is said that such functions do not generally correspond to non-linear modes because of the absence of the superposition principle in non-linear dynamics although they may constitute some approximations of them. The strength of the approaches based on the direct decomposition of measured time series is that they require no a priori characterisation of the observed non-linearities, and are generally applicable to non-stationary signals.

The Hilbert-Huang transform (HHT) [36] is potentially better than any time-frequency analysis method as it does not use a priori chosen basis for decomposition. It is therefore fully adaptive so it requires no a priori knowledge of the system or non-linearity. The HHT maps a time series into a time-frequency-amplitude distribution by a two-step procedure. In the first step, a complicated (potentially) multi-component, non-linear and non-stationary time series is decomposed into oscillatory functions, termed intrinsic mode functions (IMFs), by the empirical mode decomposition (EMD). Consequently, the instantaneous frequency and amplitude are estimated from IMFs by the Hilbert transform (HT) or other methods [27, 32, 37]. The HHT is a versatile tool which has attracted a widespread interest in many fields, including structure dynamics where it has been used for experimental and operational modal analysis [38–40], structural health monitoring [41], and parametric and non-parametric identification [42–47]. Despite not having a rigorous mathematical background, the method has a solid logical justification as evidenced by a number of successful studies. In addition, physics-based foundations of the EMD were derived in [33, 48]. Specifically, it was shown how IMFs relate to the slow-flow dynamics models derived by the complexification-averaging technique (CxA).

The objective of this paper is to show how the Hilbert-Huang transform can be used to identify the complex non-linear modes from free decay responses and to assess the accuracy of the identified modes. The possibility of identifying the CNMs by the HHT and the assessment of their accuracy have not been previously published. Firstly, it is discussed that there is a reason to believe that complex non-linear modes can be indeed identified by the HHT due to a number of similarities between the intrinsic mode functions extracted by the HHT and reduced order model of slow-flow dynamics obtained by the CNMs. This assertion is investigated numerically using a wide range of non-linear MDOF systems with different types of non-linearities. The focus of the paper is solely on free decay responses i.e. the responses of MDOF system in which several modes are excited at the same time, because it was already shown in [20] that the resonant decay response and slow-sweep responses exactly correspond to reduced order modes based on complex non-linear modes. Since the HHT does not have to be applied in those case, they are not interested from the point of view of presented topic and are not therefore described hereafter.

The paper is organised as follows: Section 2 gives a brief introduction to the theory of the Hilbert-Huang transform, complex non-linear modes, reduced order model and complexification-averaging technique. In section 2.5 the reasons supporting the existence of the relation between the HHT, CNMs and CxA are given. Then, the ability of Hilbert-Huang transform to identify complex non-linear modes is numerically assessed in section 3 using a number of MDOF non-linear systems. The experimental demonstration is also presented in section 4 where it is shown how the HHT can recover several complex non-linear modes from a single free decay response. Section 5 discusses a range of validity and implications of the obtained results and finally, the conclusions are drawn in section 6.

## 2. A brief theoretical background of the used methods, techniques and concepts

In this section a brief description of used methods, techniques and concepts is given, namely the Hilbert-Huang transform is described in section 2.1, complex non-linear modes in section 2.2, reduced order model in section 2.3 and complexification-averaging in section 2.4. Although similar description can be found

elsewhere, it was deemed appropriate to present it in this paper in order to provide enough details that are needed to discuss why the Hilbert-Huang transform should be able to identify complex non-linear modes.

### *2.1. The Hilbert-Huang transform*

The Hilbert-Huang transform (HHT) consists of two steps - the empirical mode decomposition which allows a multi-scale decomposition of a signal in terms of oscillatory functions, and a method for instantaneous frequency and amplitude estimation.

#### *2.1.1. The empirical mode decomposition*

The basic idea of the empirical mode decomposition (EMD) is to decompose a (potentially) non-stationary and non-linear time series into a set of intrinsic mode functions (IMFs), each evolving at a different characteristic time scale, in an ad hoc manner requiring no a priori system information.

The basic algorithm of the EMD can be described in the following steps [36].:

1. Identify maxima and minima of the multi-component signal $x(t)$
2. Interpolate these maxima and minima to create the upper $e_{\max}(t)$ and lower $e_{\min}(t)$ envelope
3. Compute the mean of the signal $m(t) = (e_{\min}(t) + e_{\max}(t))/2$
4. Construct the first proto-mode function $h_1(t) = x(t) - m(t)$
5. The component $h_1(t)$ is considered as the first IMF $c_1(t)$ if it satisfies two basic properties: (i) the number of extrema and zero-crossing differs by no more than one, and (ii) it has zero local mean. In practice, the latter conditions means that the mean $m(t)$ is globally smaller than a defined tolerance
6. If $h_1(t)$ is not an IMF, repeat the previous steps (referred to as a sifting process) while treating $h_1(t)$ as the signal instead of $x(t)$
7. Once the first IMF $c_1(t)$ is found, the following IMFs can be extracted from the residue $r(t) = x(t) - c_1(t)$ by repeating the process
8. The iterative process ends when the residue $r_{N_{\text{IMF}}}(t)$ (after $N_{\text{IMF}}$ IMFs have been extracted) becomes a monotonic trend or smaller than a defined tolerance

The original response $x(t)$ can be reconstructed by summarising all the IMFs $c_i(t)$ and the residue $r(t)$

$$x(t) = c_1(t) + c_2(t) + \cdots + c_{N_{\text{IMF}}}(t) + r(t). \tag{1}$$

Because the EMD explores sequentially the different time scales in the data, the components are estimated from the highest-frequency to the lowest-frequency components. That means that the lowest-frequency components may be influenced by numerical imperfections in the sifting process.

The mode mixing is of a particular concern in non-linear system identification, where is usually attempted to separate all structural modes (whose number must be known beforehand). The mode mixing refers to the fact that two or more mono-component functions with different time scales are combined or that a part of a mono-component function is estimated in a different IMF. The latter issue, also referred to as a frequency resolution of the EMD [49], can be a key limitation while using the HHT in structural dynamics where vibration modes are typically investigated. Some modes might be closer to each other than others, so care should be taken to extract all mode correctly.

The frequency resolution of the EMD was numerically and analytically studied in [49, 50]. Based on this analysis, the following criteria were established

1. Modes are separable by the EMD if

$$af \geq 1 \quad \text{and} \quad f_2 > 1.67 f_1 \tag{2}$$

2. Modes cannot be separated by the EMD if

$$af^2 \leq 1 \tag{3}$$

3. The EMD does something else and the result depends on the phase between the modes if

$$af < 1 \quad \text{and} \quad af^2 > 1 \tag{4}$$

where $f = f_2/f_1$ is the ratio of two adjacent modes ($f_2 \geq f_1$) and $a = a_2/a_1$ is the ratio of their amplitudes ($a_2 \leq a_1$). These criteria are valid for the basic algorithm of the EMD where the spline fitting is used to estimate the upper and lower envelopes, and can be used as a measure of close spaced modes. Consequently, the following discussion is only meaningful for well spaced modes (as defined by Eq. (2)), because only under this condition the modes can be extracted using the HHT.

To overcome the frequency resolution problem, several alternatives of the EMD have been developed, for instance, the application of a masking signal [48, 51], ensemble empirical mode decomposition (EEMD) [52], empirical mode decomposition using unconstrained optimisation [53] or wavelet-bounded empirical mode decomposition (WBEMD) [54]. Although the frequency resolution of the EMD can be improved, all the above mentioned advanced EMD schemes require addition insight into data, and might sometimes be difficult to use. Furthermore, for signals which can be separated by the EMD as defined by Eq. (2), the IMFs extracted by the basic EMD and by any of the advanced EMD schemes should be the same. Therefore, it is emphasised that the basic EMD used in this paper does not present a limitation with regards to the assessment of the accuracy of the estimated complex non-linear modes presented in section 3. All findings would be the same if another version of the EMD was used.

*2.1.2. Instantaneous frequency and amplitude estimation*

Having applied the EMD to a multi-component signal, the IMFs are obtained. The IMFs $c(t)$ (excluding the residuum) are single (narrow-band) frequency components, so the instantaneous frequency (IF) and amplitude (IA) can be estimated.

Traditionally, the Hilbert transform (HT) is used for this task [32, 36, 55, 56]. Once the HT $\tilde{c}(t)$ has been found, the analytic signal $z(t)$ can be derived as

$$z(t) = c(t) + \mathrm{i}\tilde{c}(t) = a(t)\mathrm{e}^{\mathrm{i}\theta(t)} \tag{5}$$

and the instantaneous amplitude $a(t)$ and instantaneous phase $\theta(t)$ can be calculated as

$$a(t) = |z(t)| = \sqrt{c^2(t) + \tilde{c}^2(t)}, \qquad \theta(t) = \arg(z(t)) = \arctan\left(\frac{\tilde{c}(t)}{c(t)}\right), \tag{6}$$

respectively. The instantaneous frequency is then defined as the time derivative of the instantaneous phase

$$f(t) = 2\pi\frac{\mathrm{d}\theta(t)}{\mathrm{d}t}. \tag{7}$$

There are several issues whist evaluating the IF using the HT as discussed in [27, 32, 37, 57]. Therefore, a zero-crossing (ZC) method [58], which is particularly appealing for its effectiveness and simplicity, is used instead. The method is particularly useful for non-parameter identification, because it usually does not require any smoothing, thereby avoiding unnecessary truncation of results. The IF is determined from the inverse of the period over one complete vibration cycle and is assigned to the zero-crossing time at the centre of this cycle

$$f(t_i) = 2\pi(t_{i+1} - t_{i-1})^{-1}. \tag{8}$$

The IA is found using the first-order polynomial interpolation of the absolute maxima of the signal. The values of these polynomials are evaluated at the zero-crossing times $t_i$. Thus, a set of discrete values $(f(t_i), a(t_i))$ is obtained. This set does not characterise the IF and IA locally (for all time), but with one cycle accuracy. On the other hand, this method removes the need to average the intra-wave modulation frequency.

*2.1.3. Non-linear modes extraction*

To comply with the CNMs definition in section 2.2, the IF and IA should be as smooth as possible so the ZC method is preferable and additional smoothing can be also recommended for experimental data. It is also necessary to note that the IF and IA should be known for all sampled time points of the original signal. Therefore, if the ZC method, which estimates the IF and IA in the discrete zero-crossing times, has been used, the IF and IA must be fitted either by polynomials or splines.

The instantaneous frequency $\omega(t) = \omega_m^k(t) = 2\pi f_m^k(t)$ and amplitude $a(t) = a_m^k(t)$ of the $m$-th vibration mode measured in $k$-th location, are used to compute the natural frequency using the Freevib algorithm [59, 60] as

$$\omega_0(t)^2 = \omega(t)^2 - \frac{\ddot{a}(t)}{a(t)} + \frac{2\dot{a}(t)^2}{a(t)^2} + \frac{\dot{a}(t)\dot{\omega}(t)}{a(t)\omega(t)}. \tag{9}$$

Often, it is possible to neglect the second-order terms and higher derivatives [32], so the natural frequency is well approximated by the measured IF, i.e. $\omega_0(t) \approx \omega(t)$.

The viscous damping rate $\delta(t) = \delta_m^k(t)$ of the $m$-th mode measured in $k$-th location can be also evaluated based on the Freevib algorithm as

$$\delta(t) = -\frac{\dot{a}(t)}{a(t)} - \frac{\dot{\omega}(t)}{2\omega(t)}. \tag{10}$$

However, it is known that the damping estimation in this way can be sometimes quite inaccurate even for the Duffing oscillator [27] due to the need to evaluate the derivatives of the amplitude and frequency. Therefore, it can be sometimes better to assess the linear viscous damping by examining the logarithmic value of the amplitude

$$d_m^k(t) = \log(a_m^k(t)). \tag{11}$$

It is well known that $d_m^k(t)$ is a straight line when the system is linear so the factor $d_m^k(t)$ indicates the deviation from the linear damping.

The fundamental amplitude of the $m$-th mode shape $|\phi_m^k(t)|$ measured in $k$-th location can be determined from the instantaneous amplitude as

$$|\phi_m^k(t)| = \frac{a_m^k(t)}{a_m^{k_0}(t)} \tag{12}$$

where $k_0$ is the index of a selected (normalisation) location. The difference between the phase angle of two modal elements $\phi_m^k(t)$ and $\phi_m^{k+1}(t)$ can be determined from

$$\angle\phi_m^k(t) = \theta_m^k(t) - \theta_m^{k+1}(t), \tag{13}$$

where $\theta(t)$ is the instantaneous phase defined by Eq. (6).

Absolute values and phase angles of all modal elements relative to the selected element can be determined and the mode shapes vector $\boldsymbol{\phi}_m = [\phi_m^1, \phi_m^2, \ldots, \phi_m^k]^{\mathrm{T}}$ assembled. Eventually, for $m$-th mode and $k$-th measured location, the frequency $\omega_m^k$, damping $\delta_m^k$ and mode shape $\boldsymbol{\phi}_m$ are identified. This set of modal properties can be used for detection and characterisation of structural non-linearities as detailed in [50], but not for their quantification as evidenced by the numerical studies performed in this paper.

*2.2. Complex non-linear modes of mechanical systems*

Consider an autonomous general dynamic system governed by

$$\mathbf{M}\ddot{\mathbf{x}}(t) + \mathbf{C}\dot{\mathbf{x}}(t) + \mathbf{K}\mathbf{x}(t) + \mathbf{f}(\mathbf{x}(t), \dot{\mathbf{x}}(t)) = \mathbf{0}, \qquad \mathbf{x}(0) = \mathbf{x}_0, \quad \dot{\mathbf{x}}(0) = \dot{\mathbf{x}}_0 \tag{14}$$

where $\mathbf{M}$ is a mass matrix, $\mathbf{C}$ is a linear damping matrix, $\mathbf{K}$ is a linear stiffness matrix, and $\mathbf{x}(t)$ is a vector of generalised coordinates. The operator $\mathbf{f}(\mathbf{x}, \dot{\mathbf{x}})$ comprises all non-linear effects, which depend on the displacement and velocity. In line with the definition of the complex non-linear mode, the motion is sought in the form [19]

$$\mathbf{x}(t) = q\Re\left\{\sum_{n=0}^{N_\mathrm{h}} \boldsymbol{\Psi}_n \mathrm{e}^{n\lambda t}\right\}, \tag{15}$$

where $q$ is a modal amplitude, $\lambda$ is a complex fundamental eigenfrequency, $n$ is the index of harmonics, and $\boldsymbol{\Psi}_n$ is a multi-harmonic complex eigenvector. Unlike in the linear modal analysis, the complex eigenvector is approximated by a truncated Fourier series, thereby having $N_h$ components. The complex fundamental eigenfrequency $\lambda$ relates to an undamped natural angular frequency $\omega_0$ and a damping ratio $\zeta$ as

$$\lambda = -\zeta\omega_0 + \mathrm{i}\omega_0\sqrt{1-\zeta^2}. \tag{16}$$

A set of unknown parameters $\lambda$, $\boldsymbol{\Psi}_0$, $\boldsymbol{\Psi}_1$, $\ldots$, $\boldsymbol{\Psi}_{N_\mathrm{h}}$ can be then regarded as amplitude-dependent modal properties.

Equation (15) is submitted to Eq. (14) and subsequent Fourier-Galerkin projection yields the following non-linear system of algebraic equations [19, 23]

$$\left[(n\lambda)^2\mathbf{M} + n\lambda\mathbf{C} + \mathbf{K}\right]\boldsymbol{\Psi}_n q + \langle \mathbf{f}(\mathbf{x}_\mathrm{p}, \dot{\mathbf{x}}_\mathrm{p}), \mathrm{e}^{\mathrm{i}n\omega_0 t}\rangle = \mathbf{0}, \quad \text{for} \quad n = 0, \ldots, N_\mathrm{h}. \tag{17}$$

For the computation of the generalised Fourier coefficients $\langle \mathbf{f}(\mathbf{x}_\mathrm{p}, \dot{\mathbf{x}}_\mathrm{p}), \mathrm{e}^{\mathrm{i}n\omega_0 t}\rangle$ of non-linear effects, a periodic formulation of displacement $\mathbf{x}_\mathrm{p}(t)$ and velocity $\dot{\mathbf{x}}_\mathrm{p}(t)$ are used (instead of the pseudo-periodic formulation defined by Eq. (15)), i.e.

$$\mathbf{x}_\mathrm{p}(t) = q\Re\left\{\sum_{n=0}^{N_\mathrm{h}} \boldsymbol{\Psi}_n \mathrm{e}^{\mathrm{i}n\omega_0 t}\right\}, \quad \dot{\mathbf{x}}_\mathrm{p}(t) = q\Re\left\{\sum_{n=0}^{N_\mathrm{h}} \mathrm{i}n\omega_0\boldsymbol{\Psi}_n \mathrm{e}^{\mathrm{i}n\omega_0 t}\right\}. \tag{18}$$

Although this periodic formulation is an approximation, it is justified [19, 22] by realising that the decrease of amplitude due to damping is relatively small within one period of motion. The periodic definition allows an effective numerical evaluation (analytical is rarely possible) of the generalised Fourier coefficients $\langle \mathbf{f}(\mathbf{x}_\mathrm{p}, \dot{\mathbf{x}}_\mathrm{p}), \mathrm{e}^{\mathrm{i}n\omega_0 t}\rangle$. The same Fourier coefficients are used in a conventional harmonic balance method so all the approaches developed therein can be used here too, including the alternating frequency/time-domain (AFT) procedure [19, 22, 61, 62] and condensation of the problem into the non-linear degrees of freedom [20].

Equation (17) cannot be solved directly because the number of unknowns is greater than the number of equations. Therefore, similarly to the linear modal analysis, normalisation conditions must be added. Several normalisation schemes have been proposed, for instance using the modal amplitude [19, 22] or kinetic energy [20]. However, the normalisation with respect to the mass matrix [23] is the most beneficial for the computation of the ROM and is also consistent with the normalisation in the linear modal analysis. Two normalisation conditions must be enforced

$$\boldsymbol{\Psi}_1^H\mathbf{M}\boldsymbol{\Psi}_1 = 1, \quad \Re\{\mathbf{t}^\mathrm{H}\boldsymbol{\Psi}_1\} = 0, \tag{19}$$

where $\mathbf{t}$ is a complex vector. The first condition represents an amplitude constrain while the second serves as a phase normalisation.

The frequency-domain solution of the non-linear eigenproblem given by Eq. (17) subjected to normalisation conditions given by Eq. (19) can be found using a Newton-Raphson method in conjunction with numerical continuation on modal amplitude such that $q \in (q_\mathrm{min}, q_\mathrm{max})$. The linear modal properties may be used as a suitable starting guess.

### *2.3. Reduced order model of slow-flow dynamics*

Having obtained the amplitude-dependent modal properties, the reduced order model of slow-flow dynamics can be derived. The slow-flow dynamics relies on the partition of the motion to fast (the frequency of oscillation) and slow dynamics (slowly varying amplitudes and phases). The ROM of slow-flow dynamics represents the system by slowly-varying variables and it is restricted to a regime where no modal interaction occurs.

The ROM based on CNMs can be derived by a modified complexification-averaging (CxA) technique [23]. The displacement and velocity are firstly transformed using complex variables as

$$\mathbf{x}(t) = q\frac{\boldsymbol{\nu}(q,\vartheta) + \boldsymbol{\nu}(q,\vartheta)^*}{2}, \quad \dot{\mathbf{x}}(t) = \mathrm{i}\Omega q\frac{\boldsymbol{\nu}(q,\vartheta) - \boldsymbol{\nu}(q,\vartheta)^*}{2}, \tag{20}$$

where the asterisk marks a complex conjugate, the manifold $\boldsymbol{\nu}(q,\vartheta)$ is generally equal to

$$\boldsymbol{\nu}(q,\vartheta)=\sum_{n=0}^{N_\mathrm{h}}\boldsymbol{\Psi}_n\mathrm{e}^{\mathrm{i}n\vartheta},\quad \vartheta=\vartheta(t)=\phi(t)+\Theta(t),\quad q=q(t), \tag{21}$$

and the angular frequency $\Omega$ is the time derivation of the fast phase $\phi(t)$. The angular frequency relates to the excitation force (the right-hand side of Eq. (14)). For an autonomous system, no excitation is present, so $\Omega=\omega_0$. Non-autonomous systems are not treated in this study so the corresponding theory is not presented and can be found in [23, 50].

An important aspect of the formulation in Eq. (21) is that the total phase $\vartheta(t)$ combines fast $\phi(t)$ and slowly $\Theta(t)$ varying components. The fast varying phase can be removed by an averaging process (detailed in [23]), and the amplitude $q(t)$ and slow phase $\Theta(t)$ can be computed from an averaged system

$$\dot{q}=-2\zeta\omega_0 q\quad\text{and}\quad\Theta=\Theta_0. \tag{22}$$

This system of non-linear differential equations can be numerically solved, provided that the initial conditions $q_0,\Theta_0$ are given.

### *2.4. Complexification-averaging technique*

The complexification-averaging (CxA) is an analytical technique that derives a slow-flow model of a system by partitioning its response into slow and fast components [30, 33, 48]. Such decomposition is possible when the response is composed by a number of well-separated dominant fast-frequency $(\omega_1,\omega_2,\ldots,\omega_N)$ components, so the response $x(t)$ can be expressed as the sum of these components

$$x(t)=y_1(t)+y_2(t)+\cdots+y_N(t). \tag{23}$$

For each component, a new complex variable is introduced

$$\psi_m(t)=\dot{y}_m(t)+\mathrm{i}\omega y_m(t)=\varphi_m\mathrm{e}^{\mathrm{i}\omega_m t},\quad m=1,2,\ldots,N \tag{24}$$

where $\mathrm{e}^{\mathrm{i}\omega_m t}$ represents the fast component and $\varphi_m$ is the slow complex component. The latter can be expressed in the polar coordinates as

$$\varphi_m=a(t)\mathrm{e}^{\mathrm{i}\Theta(t)}, \tag{25}$$

where $a(t)$ is the amplitude and $\Theta(t)$ is the slowly varying phase. By submitting Eq. (24) into the equation of motion (Eq. (14)) and applying the method of multiphase averaging, the fast-frequency components can be removed, and an averaged system governing the slow-flow dynamics obtained

$$\dot{\boldsymbol{\Phi}}=\mathbf{F}(\Phi),\quad \Phi=[\varphi_1,\varphi_2,\ldots,\varphi_N]^\mathrm{T}. \tag{26}$$

The operator $\mathbf{F}$ can become quite cumbersome even for small systems. For example, for the two-degree-of-freedom system studied in section 3.1 the operator can be found in [33]. The slowly varying amplitude and phase are then obtained by solving this averaged system. In some cases, the system can be even solved analytically and this is often the reason why the CxA is used to study non-linear systems. The application of the method is limited to small academic systems with simple polynomial non-linearities.

### *2.5. Can complex non-linear modes be estimated using the Hilbert-Huang transform?*

The previous section introduced the theoretical background of the used methods, techniques and concepts. In this section, several arguments which aim to support why the Hilbert-Huang transform should be able to estimate the complex non-linear modes will be given. The argumentation is similar to [33, 48] where it was shown that the slow-flow dynamics derived by the CxA relates to the IMFs. The relation was not proven mathematically, but rather supported by a number of similarities in the formal definitions of equations governing the CxA and HHT.

Based on the previous research it can be hypothesised that the reduced order model of slow-flow dynamics creates the link between the HHT and CNMs in the same way as between the HHT and CxA. The hypothesis is supported by the following arguments:

- The representation of the total response is consistent in all three methods (HHT, CxA and ROM based on CNMs). The HHT and CxA assume that the total response can be expressed as the sum of well separated mono-components (Eq. (1) and Eq. (23), respectively). Although the ROM is only exact in a close proximity of the mode, it has been already suggested in [23] that by superimposing the responses of different modes (which are always mono-component functions), the approximation of the total response can be obtained. Moreover, [63] presented that the concept of invariant manifold also leads approximately to the total response. Since CNMs trace trajectories on this manifold, their superposition should also lead to the approximation of the total response.

- All the methods share a common representation of dynamics. The methods partition the dynamics into slow and fast components. Although this partition is not a priori enforced in the HHT, the HHT always leads to it as evidenced by analytic signal analysis [48]. The slow-fast partition is also a key concept of the CxA and ROM based on CNMs given by Eq. (24) and Eq. (21), respectively.

- All three methods represent the signal in the complex domain, and these representations are comparable. Each method transforms a real-valued response into the complex domain. This complexification is carried out by the Hilbert transform (see Eq. (5)) in the Hilbert-Huang transform and by Eq. (24) in the CxA. It might be argued that the complexification is merely a cosmetic choice, but it was shown that these two complexifications are closely related [48]. The complexification used in the ROM based on CNMs given by Eq. (20) is essentially the same as the one used in the CxA. The difference is that the scalar complex variable in the CxA is replaced by the multi-component complex manifold in the ROM based on CNMs.

- The relation between the HHT and CxA was numerically demonstrated in [30, 33, 48] and the numerical investigation is also carried out in section 3 to assess the accuracy of the complex non-linear modes identified by the Hilbert-Huang transform. It will be also shown in section 4 that the HHT can extract several non-linear modes from an experimentally measured free decay response.

Based on these similarities, it can be hypothesised that the response of the ROM of slow-flow dynamics derived from CNMs corresponds to the IMFs obtained by the EMD. By extension, this means that the HHT can be used to identify the CNMs of mechanical systems. If the hypothesis is proven to be true, the HHT can be used as a means of non-linear modal analysis, i.e. to extract the CNMs from experimental data which would be used to quantify the system's parameters. It is not possible to mathematically prove this hypothesis due to the empirical (the HHT does not possess a rigorous mathematical background) and numerical (analytical solution for CNM and ROM cannot be obtained even for simple cases) nature of involved methods. Therefore, it is investigated using a range of numerical examples and parametric studies.

## 3. Numerical studies

In the previous section, it was argued that there are several reasons to believe that the HHT can recover CNMs from free decay responses. However, since this assertion cannot be proven mathematically, a range of numerical studies is carried out in this section.

Resonant decay responses and slow-sweep responses are not studied in this paper since it has been already shown [23, 50] that such responses matched the reduced order model exactly. On the other hand, free decay responses computed for general initial conditions are studied extensively, because they cannot be directly compared to the ROM, the EMD must be applied. A free decay is the most relevant type of data with regards to the presented topic. Free decays can be easily experimentally obtained from the hammer impact test [1] which excites several modes over a large frequency range simultaneously. Because the impulse is still finite, only the first few modes are usually excited. Numerically, similar free decays can be obtained by the numerical integration of an autonomous system subjected to the general initial conditions. The difference between the measured and computed free decay is that the computed one consists of all modes of the structure.

### 3.1. A system with cubic hardening stiffness

A simple two-degree-of-freedom system with a cubic hardening stiffness is considered. The same system, sometimes with the same parameters, has been studied in many publications, including [7, 15, 20, 23, 33, 64]. Since it is so often used, it is studied here in more detail than other systems. The system consists of two masses connected by three linear springs as depicted in Fig. 1. The non-linear (cubic hardening) stiffness is

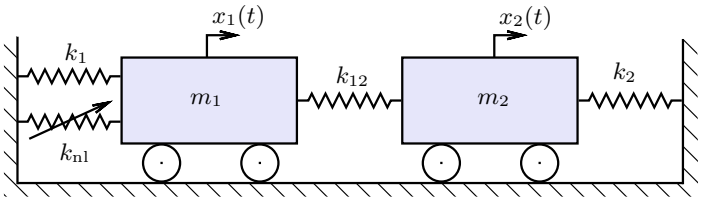


Figure 1: A two-degree-of-freedom system with a cubic hardening stiffness

located between the left mass and the ground and the system is allowed to vibrate only in the horizontal direction.

This system can be described by Eq. (14), in which

$$\mathbf{M} = \begin{bmatrix} m_1 & 0 \\ 0 & m_2 \end{bmatrix}, \quad \mathbf{K} = \begin{bmatrix} k_1 + k_{12} & -k_{12} \\ -k_{12} & k_2 + k_{12} \end{bmatrix}, \quad \mathbf{f}(\mathbf{x}, \dot{\mathbf{x}}) = \begin{bmatrix} k_{\mathrm{nl}} x_1^3 \\ 0 \end{bmatrix}, \tag{27}$$

where the parameters chosen in this part of the study are the same as in [7, 23], i.e. $m_1 = m_2 = 1\,\mathrm{kg}$, $k_1 = k_2 = k_{12} = 1\,\mathrm{N\,m^{-1}}$, $k_{\mathrm{nl}} = 0.5\,\mathrm{N\,m^{-3}}$ and modal damping ratio of 1% is also introduced.

Many more parameters variations (namely non-linear stiffness coefficients, modal damping ratios, and initial conditions) will be used in section 3.1.1 and section 3.1.2 to assess how accurate the estimated CNMs are.

The computed backbones, normalised mode shapes and a set of frequency response functions (computed using the harmonic balance method) can be seen in Fig. 2. It is clear that both modes are non-linear

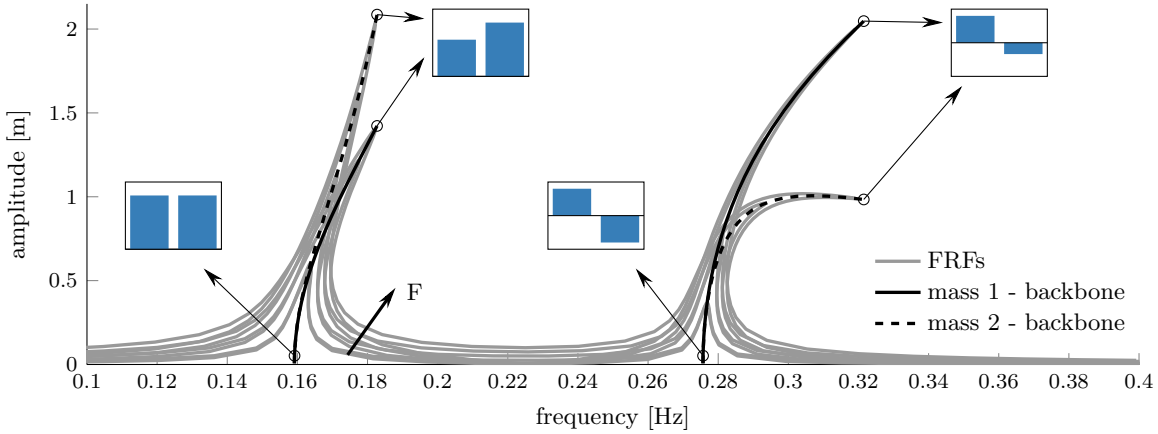


Figure 2: The computed backbones (black) and normalised mode shapes (blue) of the system with cubic hardening stiffness. The frequency response functions (grey) from both masses were added to highlight their relation to the non-linear modes.

and exhibit the hardening behaviour. The relation between the non-linear modes and FRFs is also seen, i.e. all backbones pass the maximum amplitudes of the FRFs. The computed damping (not shown) is not amplitude-depended and it is equal to the selected modal damping. The small insets in Fig. 2 depict the normalised mode shapes to emphasise the difference between the dynamics for the first and second mode. At the first mode, where both masses vibrate in phase, the amplitude of mass 1 is lower than the

amplitude of the mass 1 at high amplitudes. Whereas at the second mode, the response of the first mass becomes dominant at high amplitudes. These results are consistent with the non-linear modes presented, for example, in [7, 23]. The backbones are used to compute the ROM of slow-flow dynamics which is then compared with the extracted IMFs. It should be noted that the ratio of the natural frequencies of the system, $f_1 = 0.1591\,\text{Hz}$ and $f_2 = 0.2757\,\text{Hz}$, is equal to 1.73. It is therefore close to the theoretical mode mixing limit set by Eq. (2) so it is possible that some mode mixing may occur, but it should not significantly impact the resulting IMFs.

Here, a detailed comparison (including the comparison with the CxA from [33, 48]) is made for the parameters of the nominal system listed above. To compute the free decay response, the initial displacement $\mathbf{x}_0 = [1\,\text{m}, 0]^T$ and zero velocity are used. The computed data are shown in Fig. 3. It can be seen that

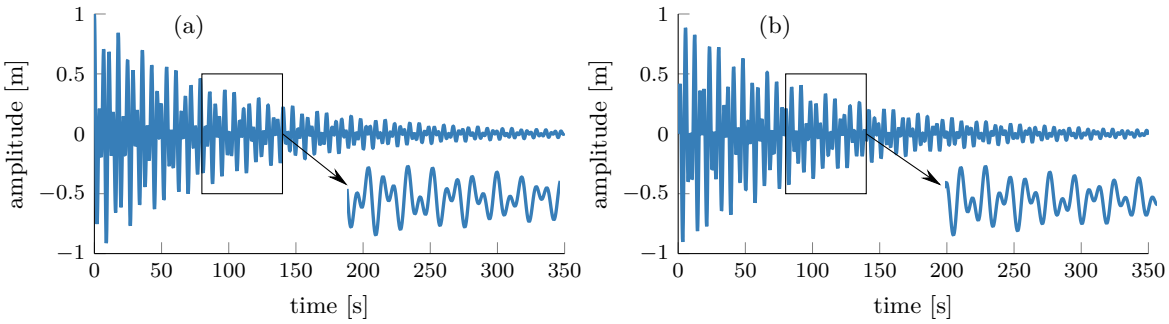


Figure 3: Computed free decay response of the system with cubic hardening stiffness: (a) mass 1 and (b) mass 2

both responses consist of two modes of different frequencies, so the EMD is necessary to separate the modes from each other. The basic algorithm of the EMD described in section 2.1.1 was used and the resulting IMFs (there were no spurious IMFs extracted) are shown in Fig. 4. Unlike the original signal, the IMFs

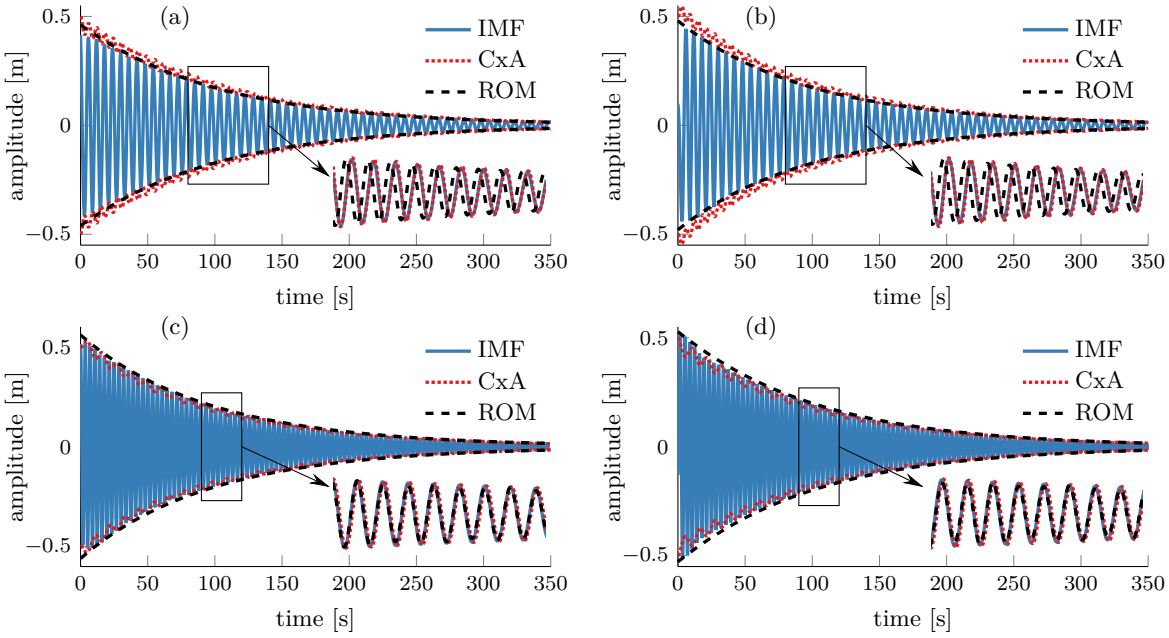


Figure 4: Comparison of the IMFs and ROM for the system with cubic hardening stiffness: (a) first mode, mass 1, (b) first mode, mass 2, (c) second mode, mass 1, and (d) second mode, mass 2

are single frequency components. Therefore, they look very similar to resonant decay responses. Despite

the use of the basic algorithm of the EMD, no numerical problems can be observed, i.e. there are no end effects and modes are clearly separated and therefore it can be safely assumed that the use of advanced EMD schemes for mode mixing problem resolving (masking signal, EEMA, WBEMD or any other method) would not change the IMFs.

For the same initial conditions, the ROM of slow-flow dynamics derived from the CNMs and by the CxA are also shown in Fig. 4. Overall, all three responses match for both masses and both modes. However, there are a few small differences that are worth noting. Firstly, the first mode response of the ROM is slightly different than the response of the CxA and the IMFs. The amplitude (envelope) is captured correctly, but the frequency appears to be slightly lower at the beginning which cumulatively causes an apparent shift of the ROM response (see the inset in Fig. 4(a) and Fig. 4(b)). Secondly, despite the fact that the amplitude of the CxA responses corresponds well to the maxima of the IMFs, the amplitude appears to fluctuate in between extrema. Similar, but not so severe, fluctuation of the amplitude can also be seen in [33]. Nevertheless, the final CxA response, seen in the insets in Fig. 4, appears to match the IMFs very well, with no shift in the frequency or mismatch in the amplitude.

The Hilbert spectrum of the IMFs together with the ROM frequency is shown in Fig. 5. It can be seen

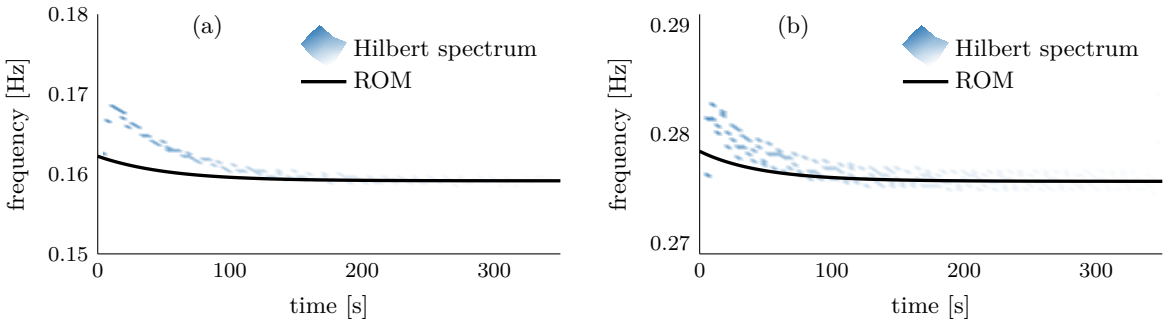


Figure 5: The Hilbert spectrum of the two-degree-of-freedom system with the cubic hardening non-linearity: (a) the first mode and (b) the second mode

that the ROM indeed predicted the frequency lower than the frequency which is estimated by the HHT. The differences in frequency are less than 5 % for both modes.

Based on the presented cases, it appears that the Hilbert-Huang transform is indeed able to recover the complex non-linear modes from the free decay responses. However, it is also obvious that the match between theoretical and identified natural frequency is not exact. It appears that the match of the IMFs and ROM is less accurate for the first mode due to the slightly lower frequency of the ROM response. This suggests that the identification results can be only successfully used for detection and characterisation of non-linearities, but would fail to lead to correct quantification. However, since a single set of parameters and initial conditions has been studied so far this conclusion is not well supported. In order to further support the conclusions and improve the understanding of the difference observed between the IMFs and ROM, two parametric studies are conducted.

*3.1.1. Parametric study 1 - The influence of non-linear stiffness and modal damping ratio*

It would be ideal to vary all parameters of the system and observe how accurate the estimated complex non-linear modes or extracted reduced order models are. However, it would be practically impossible to visualise and evaluate the results in a systematic manner. Therefore, the focus in this section is on the influence of the modal damping ratio in a range $\zeta \in [0, 3]$ % and non-linear stiffness coefficient $k_{\mathrm{nl}} \in [0, 2]$ N m$^{-3}$. These two parameters have been previously observed to have a significant influence on the ROM of a single mode of vibration [23]. The parameters of the under-lying conservative system and the initial conditions have not been changed. The parametric study is conducted in an automatic manner so the performance of the EMD is not explicitly verified for each case. However, the correspondence of the ROM

and IMFs is evaluated in such a way that possible end effects, which may be caused by spline fitting during EMD, will not influence the results.

In order to evaluate the correspondence of the ROM and IMFs, the correlation coefficient $C_m^{(k)}$ between the IMF and the response of the ROM of the $k$-th mass and $m$-th vibration mode has been calculated. The correlation coefficient $C_m^{(k)}$ is equal to one if there is no difference between the IMFs and ROM and zero if the IMF and ROM are not correlated. The correlation coefficient takes into account the whole response so it captures the information about the amplitude and frequency at the same time.

Comparing whole responses would not be practical, due to significant changes in the frequency and decay rate caused by the different stiffness and damping. Moreover, the end effects of the EMD could influence the resulting correlation coefficient too. Therefore, in order to perform a meaningful comparison, first two periods of the response were removed and the next five periods were used for the computation of $C_m^{(k)}$.

In total, 77 systems for different values of non-linear stiffness coefficient and damping ratio have been investigated. In each case, four correlation coefficients, corresponding to two modes and two masses, were obtained. To evaluate an overall match between the estimated IMFs and computed ROM, these four coefficients were averaged. The results of the first parametric study are shown in Fig. 6. This surface covers

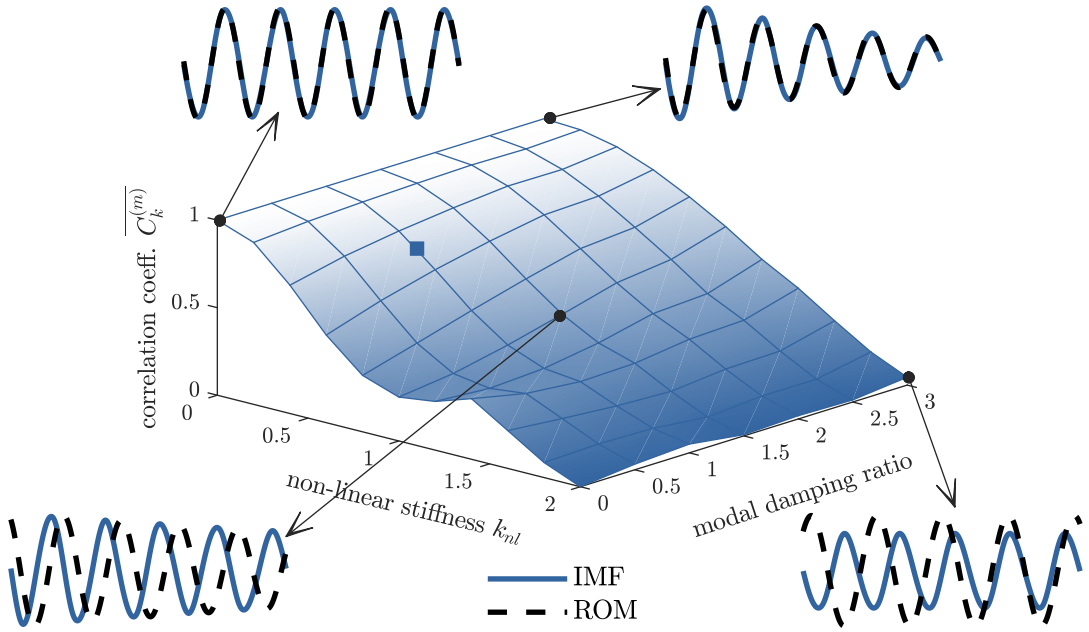


Figure 6: Parametric study 1: the influence of the non-linear stiffness and modal damping ratio on the comparison between the IMFs and ROM visualised using the correlation coefficient. The blue square represents the configuration of the system studied in detail in section 3.1.

a number of systems, ranging from linear to strongly non-linear ($k_{\mathrm{nl}} \in [0, 2]\ \mathrm{N\,m^{-3}}$) with no to high modal damping ($\zeta \in [0, 3]$ %). The insets contain the direct comparison of the IMFs and ROM of the first mode and first mass (similarly to Fig. 4(a)). This comparison in the insets is made for the five periods that have been used to evaluate the correlation coefficient. It should be noted that the insets represent the worst observed cases since the match for the second mode is usually much better (similarly to Fig. 4).

It is clear from Fig. 6 that for linear systems the match between the IMFs and ROM is perfect and independent of the damping. On the other hand, for non-linear systems, the correlation coefficient is not equal to one and the damping, albeit linear, also influences its value. A trend can be observed - the correlation decreases with the increasing stiffness and decreasing damping. This means that the overall correspondence between the IMFs and ROM (and by extension the IF and IA, and CNMs) is not so good for lightly damped, strongly non-linear systems. This is despite the fact that the CMNs is better suited for

lightly damped system due to periodic formulation in Eq. (18). The reason for higher correlation between the IMF and ROM for highly damped system is not known. The insets in Fig. 6 show that in a majority of cases, the discrepancies between the IMFs and ROM originate in the difference between the frequencies, whereas the amplitudes match reasonably well. This is not true for the largest values of non-linear stiffness and lowest damping. In that case, even the amplitudes do not match very well as visualised for $k_{\mathrm{nl}} = 2\,\mathrm{N\,m^{-3}}$ and $\zeta = 0\,\%$ (the upper right inset in Fig. 6).

To summarise the first parametric study, it can be stated that there is no exact correspondence between the IMFs and ROM. Despite this the IMFs and ROM exhibit the same qualitative features (shift in the frequency, decrease in amplitude) while the quantitative error may be significant in some cases. This finding suggests that the HHT is not able to estimate the CNMs accurately, only approximately.

*3.1.2. Parametric study 2 - The influence of initial conditions*

The free decay response of a system is significantly influenced not only by the system parameters, but also by the initial conditions. For this reason, the influence of the initial displacements on the relation between the IMFs and ROM is investigated in a range $x_1(0) \in [0,\ 1.5]$ m and $x_2(0) \in [0,\ 1.5]$ m. The other parameters of the system were the same as in the original configuration and the initial velocity was set to zero. The analysis has been conducted in the same manner to the previous parametric study, i.e. the time response was calculated, the EMD applied and the IMFs compared to the ROM by means of the correlation coefficient.

Because both initial conditions varied, it was not always possible to decompose the response into two IMFs for each mass. Sometimes, only a resonant decay response is excited whereas in some cases, the contribution of one of the modes is so weak that the EMD cannot extract both modes property. Therefore, for the evaluation using the correlation coefficient, only the first mode from the first mass is considered, i.e. only the coefficient $C_1^{(1)}$ is determined. Furthermore, before attempting the EMD, it was evaluated whether it can obtain the proper IMFs. This was achieved by applying the following process - the FFT was applied, the fundamental frequency and corresponding amplitude of both modes found, and the criteria given by Eqs. (2)-(4) evaluated. When it was found that the EMD can separate the modes clearly, the ROM of the first mass was compared with the last IMF, which corresponds to the first mode. On the other hand, when it was determined that the EMD cannot separate the modes, the response of the system, which is very close to a resonant decay response, was directly compared with the ROM of the first mode. The cases where the EMD cannot clearly separate the modes, but changes the original signal were not considered.

In total, 10200 systems for different values of the initial displacements have been investigated. The parametric study yielded the surface shown in Fig. 7 which covers the area around the first mode. Three well separated regions can be recognised, specifically, in region (1) the EMD returns 2 correct modes, in region (2) the EMD changes the signal, but cannot give correct modes, and in region (3) the EMD cannot decompose the signal at all without using the masking signal or EEMD as discussed in section 2.1.1. The theoretical lines corresponding to the criteria from Eqs. (2)-(4) are also shown. In addition, the dashed line, passing roughly through the centre of the graph in region (3), indicates the initial conditions which lead to the excitation of a resonant decay response of the first mode only.

In region (1), the correlation coefficient monotonically decreases with increasing initial conditions, indicating that the match between the IMFs and ROM is not so good for high initial displacements. This is in line with the previous observation, since the increase of initial conditions essentially leads to stronger non-linear behaviour for higher amplitude at the beginning of the signal. It therefore indicates that the match between the IMFs and ROM is less accurate for strong non-linearity. Most of the discrepancies between the IMFs and ROM originate in the frequency, whereas the amplitude appears to match well. This can be nicely observed in the insets in Fig. 7 for $\mathbf{x}_0 = [0.4,\ 1.5]$m (upper left) and $\mathbf{x}_0 = [1.5,\ 0.6]$m (bottom right). In both cases, the amplitude match very well while the frequency causes an apparent shift of the ROM response. As expected, the correlation coefficient approaches one for very low initial conditions. This is due to the fact, that for such a low initial displacement, the system basically behaves as a linear one. The blue square in Fig. 7 marks the configuration of the system studied previously in Fig. 4. Similar conclusions can be drawn for a number of systems in this parametric study too. It can be again argued that the insets represent the worst possible cases of the correspondence between the IMFs and ROM.

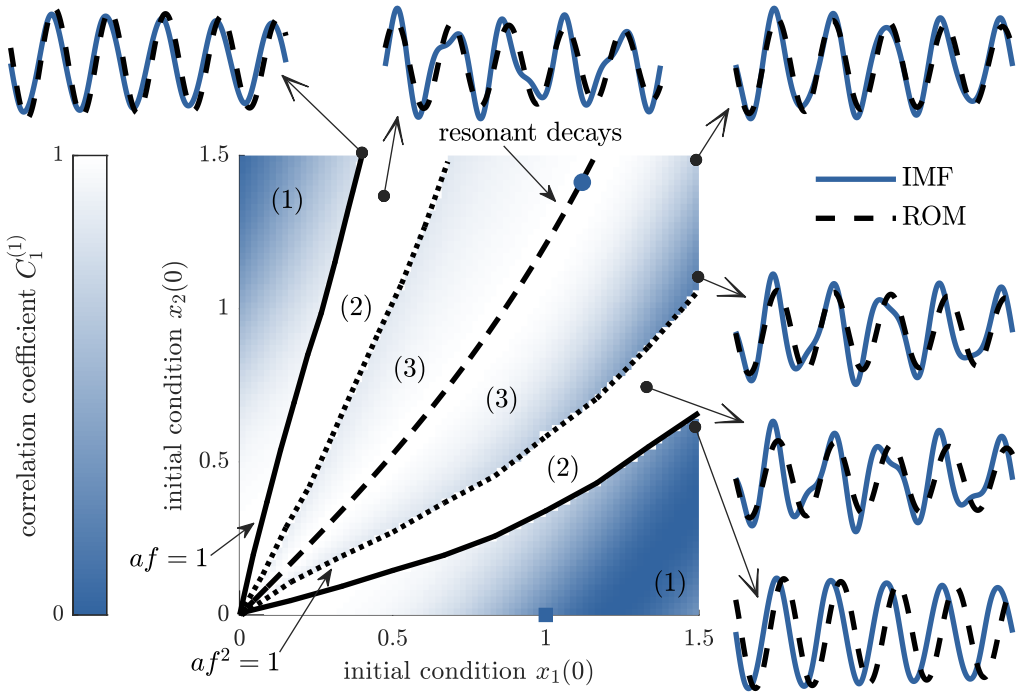


Figure 7: Parametric study 2: the influence of the initial displacement on the relation between the IMFs and ROM visualised using correlation coefficient. The thick black lines represent the criteria for the frequency resolution of the EMD described in section 2.1.1 and divide the graph into three regions: (1) the EMD separated the vibration modes, (2) the EMD was not applied since its effect to the signal is uncertain, and (3) the EMD cannot separate the modes so the simulated signals were directly compared to the ROM computed from the complex non-linear modes. The blue square represents the configuration of the system studied in section 3.1 in detail. The resonant decay response which would be computed from the initial conditions marked by the blue dot was presented in [23, 50] as an example of the exact match between the time-domain response and reduced order model.

In region (3), in which the EMD neither separates the modes, nor changes the original signal, the first observation is that for the low initial displacements ($< 0.5$ m), the match of the response of the system and the ROM is very good, despite the fact that no EMD was needed. For higher initial conditions, the match is extremely good when the system is released with the initial conditions corresponding to the first mode (dashed line in Fig. 7), or in a close proximity of these conditions. The example of the exact match for the initial conditions that are indicated by the blue dot in Fig. 7 was given in [23]. Region (3) suggests that even if the initial conditions are not adjusted perfectly for resonant decay measurements in an experimental setting, it may still be possible to capture a resonant decay response of a considered mode exactly. However, it must be noted that for the higher initial conditions, the ROM ceases to exist due to modal interactions [23] so the comparison with the IMF is no longer possible. In the rest of region (3), the correlation coefficient $C_1^{(1)}$ decreases with the distance from the resonant decay response. This is in line with the fact that the accuracy of the HHT-estimated CNMs is violated when the IMF is not extracted or measured appropriately as well as the fact that the ROM can capture only non-linear modal responses accurately. Most of the discrepancies seen between the IMFs and ROM are caused by mismatch in the frequency, whereas the total amplitude seems to be captured correctly. For example, the insets in Fig. 7 for $\mathbf{x}_0 = [1.5, 1.5]$m (upper right corner) and $\mathbf{x}_0 = [1.5, 1.1]$m (under the legend) show that the overall amplitude is correctly captured, whereas the frequency seems to have a significant modulated component that causes the mismatch of the responses. Based on these findings, it can be concluded that the response of the first mode can still be approximated by the ROM of slow-flow dynamics, even if it has not been measured with the exact initial conditions of a considered mode.

In region (2), no correlation coefficient has been evaluated, because the EMD may lead to spurious IMFs

and directly measured responses are far from the resonant decay response. It can be seen in the insets for $\mathbf{x}_0 = [0.4,\ 1.4]$m (right) and $\mathbf{x}_0 = [1.4,\ 0.8]$m (above) that the time domain signal is composed of two modes, but these cannot be separated by the EMD due to a lack of local extrema. When showing the ROM in the same inserts, it is revealed that the qualitative difference between two signals is quite significant, thereby making any comparison meaningless.

### *3.2. A system with quadratic damping*

A simple two-degree-of-freedom system with non-linear quadratic damping is considered in this section. The system has the same spatial layout as the system in Fig. 1, but the cubic spring has been replaced by a non-linear dashpot. Such system can be therefore described by Eq. (14) with mass and stiffness matrix given by Eq. (27), but the non-linear restoring force now reads

$$\mathbf{f}(\mathbf{x}, \dot{\mathbf{x}}) = \begin{bmatrix} c_{\mathrm{nl}} \dot{x}_1 |\dot{x}_1| \\ 0 \end{bmatrix}, \tag{28}$$

where $c_{\mathrm{nl}}$ is the coefficient of the quadratic damping. The parameters of the system chosen in this study were $m_1 = m_2 = 1\,\mathrm{kg}$, $k_1 = 0.1\,\mathrm{N\,m^{-1}}, k_2 = k_{12} = 1\,\mathrm{N\,m^{-1}}$, $c_{\mathrm{nl}} = 0.5\,\mathrm{N\,s\,m^{-1}}$ and linear modal damping of 1 % was introduced as well. Due to the presence of the non-linear damping, this case cannot be studied by the classical definition of non-linear normal modes (NNMs), which are applicable only to conservative systems.

The computed backbones, damping curves, normalised mode shapes and a set of frequency response functions can be seen in Fig. 8. Despite the fact that no stiffness non-linearity has been added to the

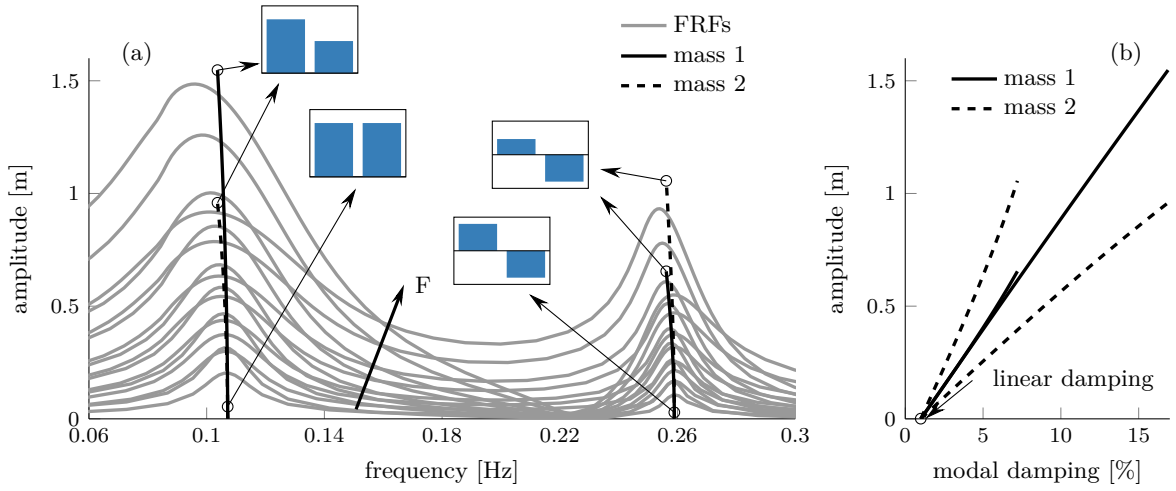


Figure 8: The system with quadratic damping: (a) backbones, normalised mode shapes and frequency response functions, and (b) the modal damping

system, the backbones lean slightly to the left. This amplitude-dependent nature of the resonance frequency due to the quadratic damping has also been reported in [65]. Unlike in Fig. 2, the backbones do not pass through the peak of the FRFs exactly. The validity of the FRFs and backbones have been verified by convergence studies for different number of harmonics, but the results remained unchanged. The difference between the peaks of FRFs and backbones is less than 8 % in all cases and it is most likely caused by the used periodic formulation in Eq. (17). This formulation assumes that the decrease in the amplitude due to damping is relatively small. However, it will be seen in this section that this assumption is not well satisfied for this system, thereby probably causing a slight mismatch between the FRFs and the backbones.

Unlike in the previous system with cubic hardening non-linearity, the damping curves are strongly dependent on the amplitude as seen in Fig. 8(b). The damping increases non-proportionally with the increasing

amplitude, which is in line with [65] in which a similar linearity plot of an SDOF system with quadratic damping was presented. The non-linear behaviour of the frequency and damping can be also observed from the FRFs in Fig. 8(a). The FRFs are flat due to damping and their peaks are slightly shifted to the left. As can be seen in the insets in Fig. 8, the non-linear mode shapes exhibit the same behaviour as for the previous system (Fig. 2), i.e. at the first mode, the motion of mass 1 becomes prominent at high amplitudes, whereas at the second mode, mass 2 has larger displacements.

The free decays shown in Fig. 9 were computed for the initial displacement $\mathbf{x}_0 = [1, 0]^T$ and zero initial velocities. It can be seen that both responses consist of both modes. The overall character of the response

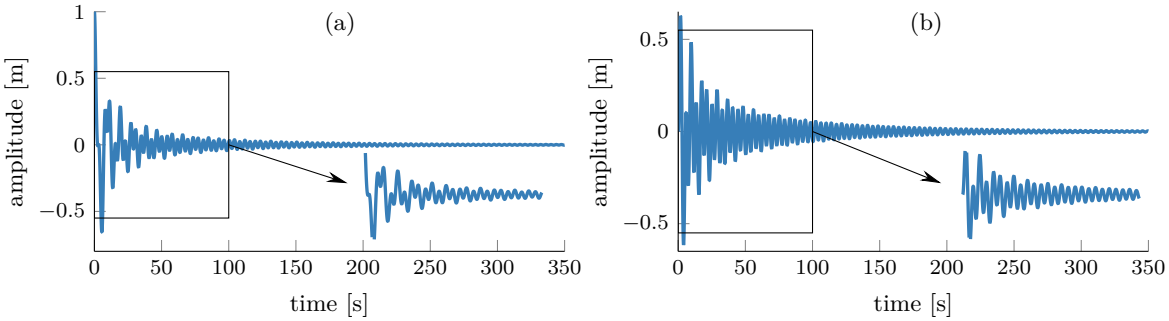


Figure 9: Computed free decay response of the system with quadratic damping: (a) mass 1 and (b) mass 2

is significantly different compared to Fig. 3 for the system with cubic hardening stiffness. The presence of strong damping effects is prominent at the beginning of the signal where a dramatic decrease in the amplitude can be clearly seen. Despite the fact that mass 1 was released from 1 m, its amplitude was less than 0.4 m in the second period of vibration. The damping is much stronger at the beginning, but becomes weaker toward the end of the signal as can be seen from the gradual decay rate after first 20 s.

Because the signals consist of both vibration modes, they must be decomposed into the IMFs by the EMD. The IMFs are shown in Fig. 10. Unlike the original signal, the IMFs seemingly look as responses of an SDOF system or resonant decay responses. There are several numerical imperfections which originated in the EMD that can be observed in the IMFs. The unwanted end-effects caused by the spline fitting in the EMD at the beginning of the signal can be seen in Fig. 10(c). This end effect is not significant and does not influence the rest of the IMFs as seen in the inset.

For the same initial conditions, the ROM has been computed and the results are shown in Fig. 10 as well. As can be seen, the match of the ROM and IMFs is very good, apart from the beginning, for the second mode (Fig. 10(c) and Fig. 10(d)) where both amplitude and frequency match to each other. On the other hand, the match of amplitudes is not so good for the first mode (Fig. 10(a) and Fig. 10(b)) where the amplitude of the IMFs seems to be decreasing more rapidly at the beginning of the time interval. In spite of the difference in the amplitude, the frequency of the ROM matches the IMF very well. As in the previous example, the match between the IMFs and ROM is not perfect, but both of them still display a certain level of similarities. This again means that the CNMs estimated from these IMFs cannot match to the theoretical ones accurately.

### *3.3. A cantilever beam with geometric non-linearity*

For the last demonstration, a numerical model of a cantilever beam is used. This model is based on the École Centrale de Lyon (ECL) benchmark, which was originally designed for the comparison of non-linear system identification methods [24, 66] and has been intensively used ever since, e.g. for numerical [14] and experimental demonstration of NNMs [15]. The ECL benchmark consists of a long cantilever beam with a geometric non-linearity introduced by a much thinner beam at one end.

The finite element (FE) model of the beam is graphically represented in Fig. 11. The main beam was discretised by 10 Euler-Bernoulli beam elements and the effect of the thin beam was introduced by the cubic hardening spring at the tip of the main beam. The geometrical and mechanical properties of the beam were

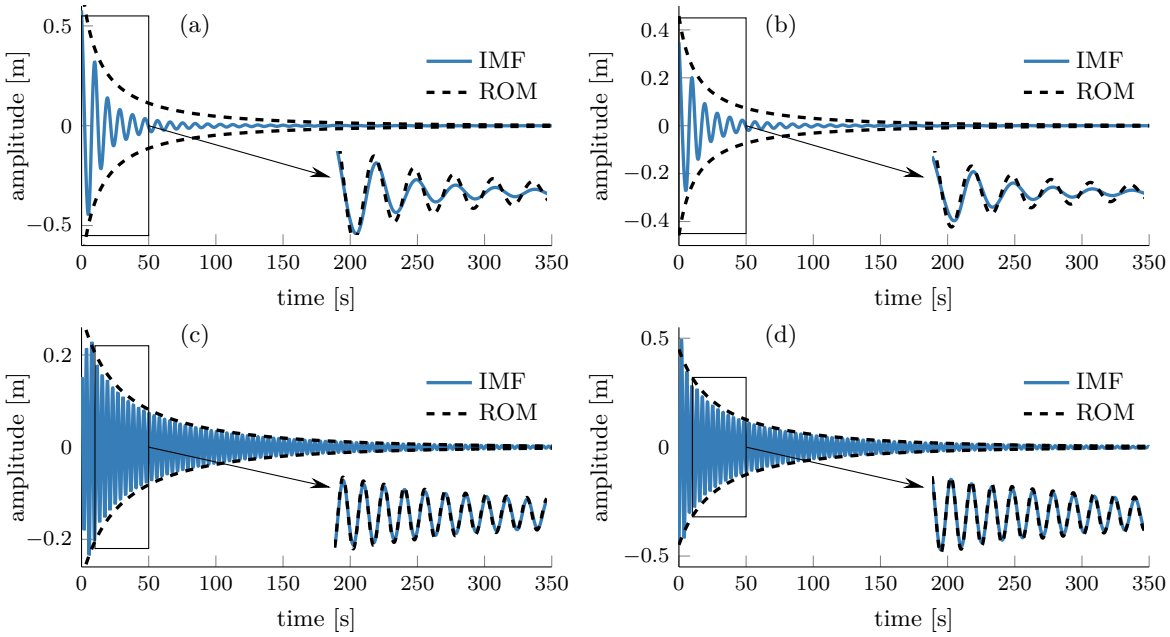


Figure 10: Comparison of the IMFs and ROM for the system with quadratic damping: (a) first mode, mass 1, (b) first mode, mass 2, (c) second mode, mass 1, and (d) second mode, mass 2

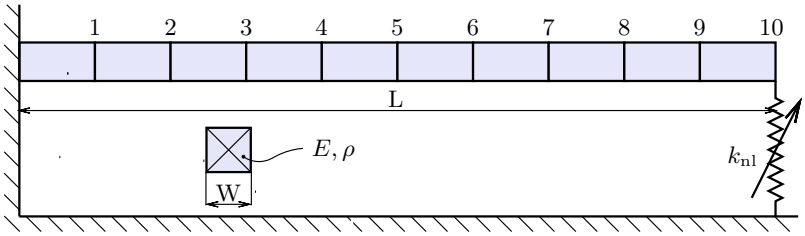


Figure 11: A model of the cantilever beam with geometric non-linearity

$L = 0.7\,\mathrm{m}$, $W = 0.014\,\mathrm{m}$, $E = 2.1 \times 10^{11}\,\mathrm{Pa}$, $\rho = 7800\,\mathrm{kg\,m^{-3}}$ and the system was allowed to vibrate only in the vertical direction.

The system can be modelled based on the FE model using Eq. (14), in which the mass $\mathbf{M}$ and stiffness $\mathbf{K}$ were assembled by a standard FE procedure using beam elements (the vector $\mathbf{x}$ consists of displacements and rotations). Unlike in the previous cases, the linear viscous damping was introduced using Rayleigh's proportional damping model, i.e. $\mathbf{C} = \alpha\mathbf{M} + \beta\mathbf{K}$, with $\alpha = 2$ and $\beta = 1 \times 10^{-8}$. The vector of non-linear restoring forces consisted of a single non-zero element corresponding to the displacement DOF of node 10 with the chosen cubic hardening stiffness coefficient $k_{\mathrm{nl}} = 1 \times 10^{8}\,\mathrm{N\,m^{-3}}$.

The computed backbones, normalised mode shapes and a set of frequency response functions can be seen in Fig. 12. Three harmonics were again used in both non-linear modal analysis and harmonic balance method since the convergence analysis indicated that this number was sufficient. It can be seen that both displayed modes are non-linear, exhibiting the hardening behaviour. The backbones pass correctly the peaks of the FRFs and the computed damping (not shown) is not amplitude-dependent. The first and second mode shapes, which are normalised so that the amplitude of node 10 is equal to 1 and -1, respectively, are depicted in Fig. 12(c) and Fig. 12(d). It can be seen that both mode shapes change with the increasing amplitude. However, the change is not so dramatic as in the simpler systems that were previously studied. These results are consistent with the computational studies of the ECL benchmark using NNMs in [14, 16, 67] and will

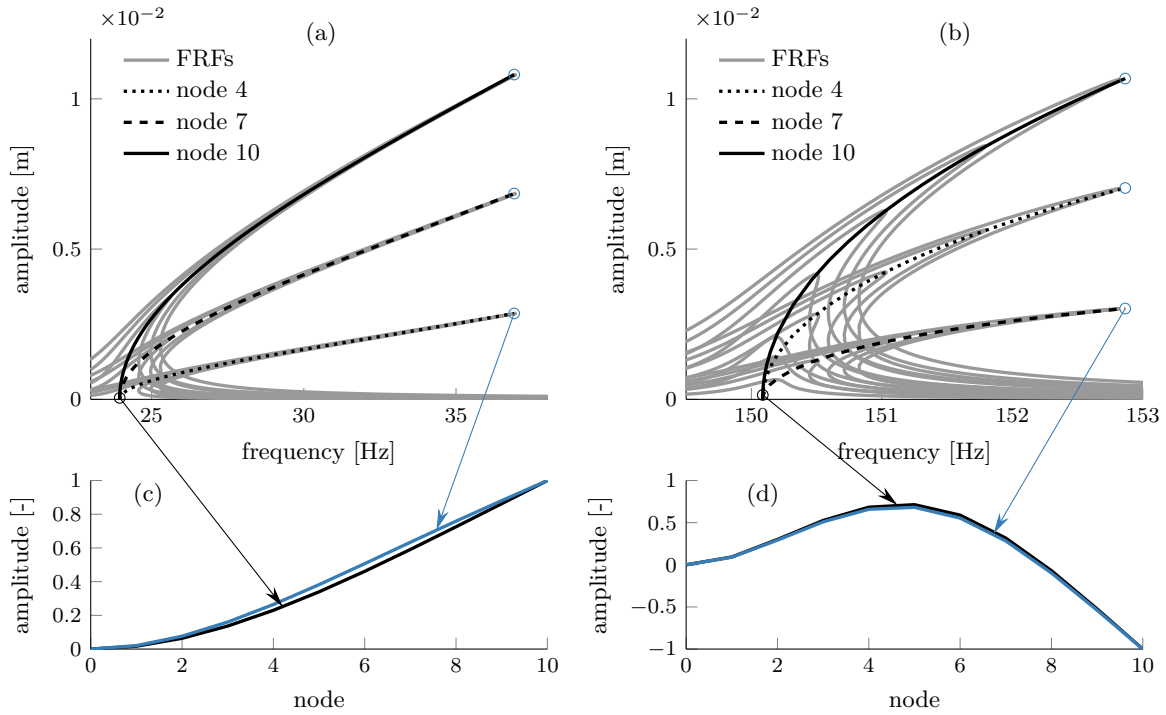


Figure 12: The cantilever beam with geometric non-linearity: (a) computed backbones and frequency response functions of the first mode, (b) computed backbones and frequency response functions of the second mode, (c) the first mode shape, and (d) the second mode shape

be also obtained experimentally in section 4.

The response of the system was simulated for the initial displacement of the tip of the beam $x_{10}(0) = 0.1\,\mathrm{m}$ and the free decays obtained can be seen in Fig. 13. The results are herein presented for the vertical

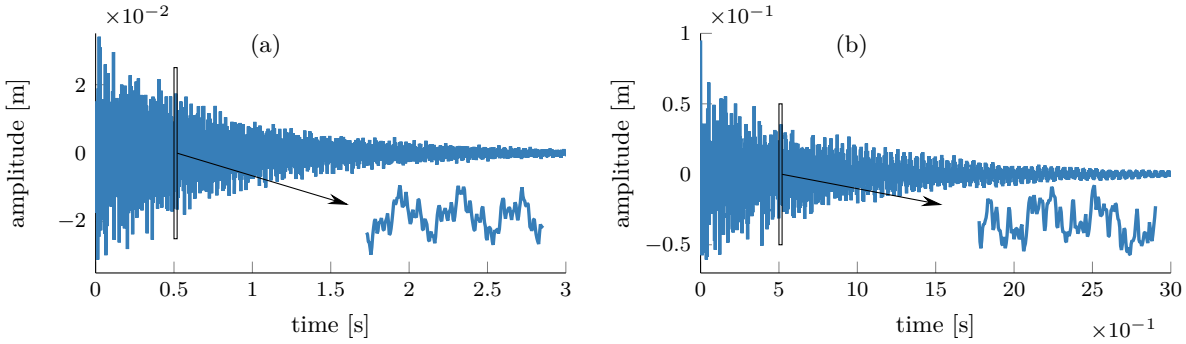


Figure 13: Free decay responses of the cantilever beam with geometric non-linearity: (a) node 4, (b) node 10

displacements of two nodes - node no. 4, which is close to the middle of the beam, and node no. 10, which is at the tip of the beam and to which the non-linear spring is attached. As can be seen, both responses exhibit multiple modes, thereby preventing direct estimation of the IF and IA.

After the application of the EMD, several IMFs have been obtained. In Fig. 14, only the last two IMFs, which correspond to the first and second mode, are shown. Because these two IMFs are the last ones that were extracted using the EMD (excluding the final trend), the quality of them is not so high as in the previous cases. A noisy appearance is caused by the imperfections in the shifting process. It will be observed

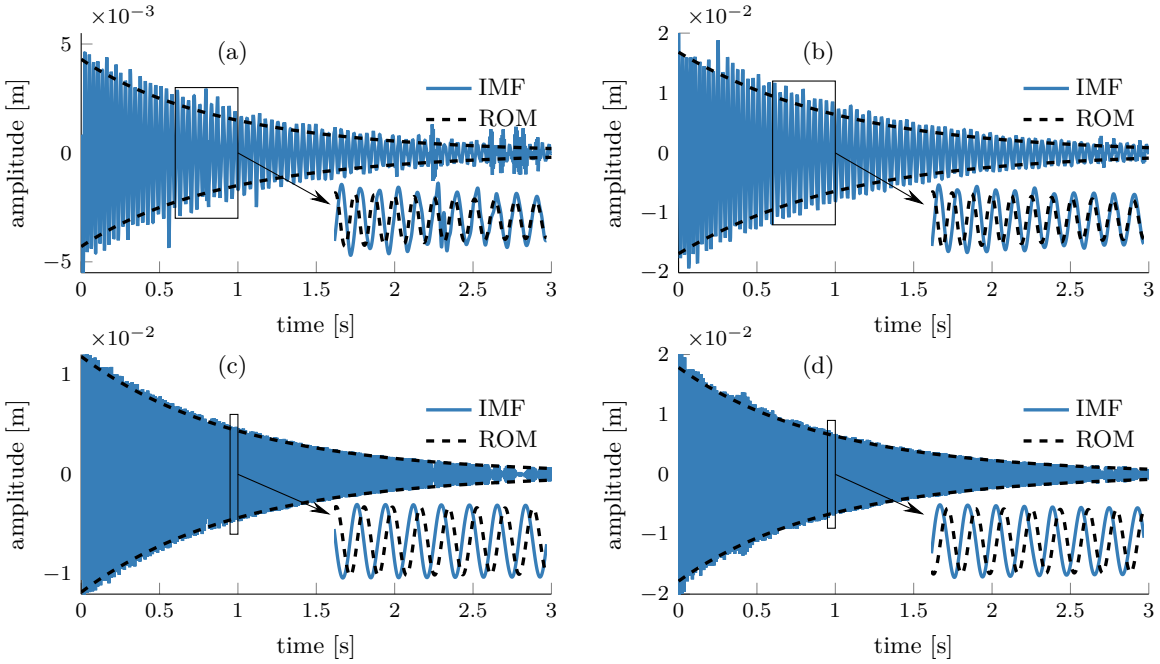


Figure 14: Comparison of the IMFs and ROM for the cantilever beam with geometric non-linearity: (a) first mode, node 4, (b) first mode, node 10, (c) second mode, node 4, and (d) second mode, node 10

in section 4 that the EMD performs much better for experimental data. The reason is that when computing free decay by setting initial conditions instead of applying a short time impact, all structural modes are excited and must therefore be separated from the data. On the other hand, if real impulse excitation is applied, only a first few modes are excited, allowing the EMD to perform better. Nevertheless, it is clear that the IMFs in Fig. 14 are not multi-component signals any more and that they vibrate with different time scales.

For the same initial conditions, the ROM has been computed and is shown in Fig. 14 as well. Although the match of IMFs and ROM is not so good as in the previous cases, the amplitudes seem to match quite well. The local discrepancies in the amplitudes are believed to be mainly caused by the imperfections of the EMD. The match in terms of frequency is acceptable as well. However, some small differences can still be observed, indicating slightly higher frequency of the IMFs.

To further investigate the difference between the ROM and IMFs in this case, the IF and IA are estimated using the ZC method. The results are shown in the Hilbert spectrum (time-frequency-amplitude map [68]) in Fig. 15. The Hilbert spectrum of the first mode (Fig. 15(a)) shows that the estimated IF is indeed higher than the frequency predicted by the ROM at the beginning of the signal. The difference is approximately 10 %. On the other hand, the frequency of the second mode predicted by the ROM fits the IF very well. It can be seen that the second mode does not display such strong non-linear behaviour. The Hilbert spectrum is not so clear, especially for the lower amplitudes. This is believed to be caused by the numerical imperfections in the EMD.

A reasonably good match between the response of the ROM and IMFs in Fig. 14, and the frequency predicted by the ROM and the estimated IF in Fig. 15 further supports the assertion that the HHT can be used to estimate the CNMs. However, due to the quantitative difference in the frequency, the identified CNMs cannot be accurately used for quantification of system's parameters.

*Summary of numerical studies*

The numerical studies performed in this section yielded an important conclusion - the intrinsic mode function relate to the reduced order model of slow-flow dynamics obtained from complex non-linear modes

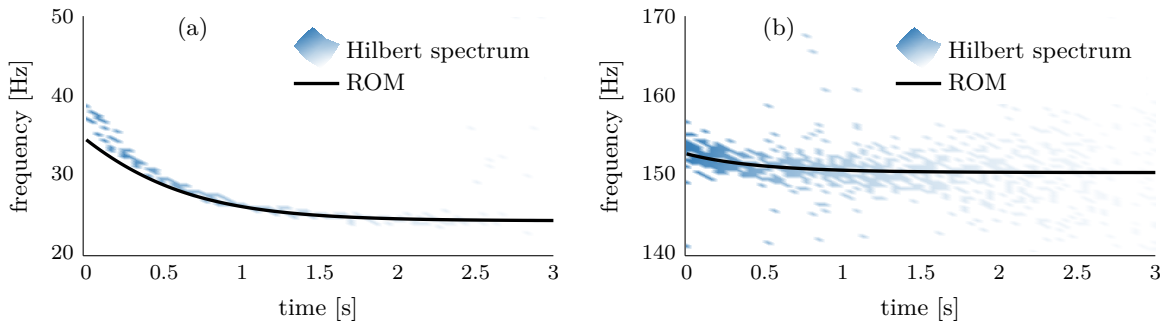


Figure 15: The Hilbert spectrum of the cantilever beam with geometric non-linearity: (a) the first mode (b) the second mode

only approximately. This finding means that the ability of the HHT with regards to quantification of structural non-linearities using the CNMs is very limited although detection and characterisation in a non-parametric manner is possible.

## 4. Experimental demonstration

The previous section showed that the CNMs estimated by the HHT should be used only for detection and characterisation of non-linearities, not for their quantification. This was shown using the comparison of the IMFs and ROM for a number of numerical systems. In this section, it will be shown that the CNMs can be also estimated from an experimentally acquired free decay response of the ECL benchmark.

The ECL benchmark was designed to compare non-linear system identification methods [66] and has been extensively used in the past 15 years for both numerical and experimental studies. Many non-linear system identification methods have been applied to this benchmark, including conditioned reverse path method [69], proper orthogonal decomposition [70], wavelet transform [71], normal non-linear modes [15, 67] and model updating [72].

The ECL benchmark consists of a main long cantilever beam with a thin short beam attached to its end. The thin beam is also clamped and introduces a strong geometric non-linearity. The nominal dimensions of the beams are the same as in [15, 67]. The main beam is 0.7 m long, 0.014 m wide and 0.014 m thick while the thin beam is only 0.04 m long, 0.014 m wide and 0.0005 m thick. Both beams are made of steel with nominal Young's modulus $E = 2.1 \times 10^{11}$ Pa and density $\rho = 7800\,\mathrm{kg\,m^{-3}}$.

The experimental set-up is shown in Fig. 16. The connection of the thin and main beam is realised through a simple bolted joint. The care was taken to manufacture this connection as accurately as possible in order to minimise any friction effects. The dynamic response to impact excitation is measured by three accelerometers placed at node 4, 7 and 10. The shaker seen in Fig. 16 was not attached to the beam during the measurement.

Prior to extraction of the non-liner modes, the linear modal analysis was conducted to find natural frequencies and damping ratios. The linear modal analysis was performed on the main beam only, i.e. without the thin beam attached. The accelerometer on the tip of the beam (in node 10) was used and the impact hammer excitation was applied to measure the frequency response functions (FRFs). The FRFs were processed the least-square complex frequency (LSCF) estimator [73] which estimated three natural frequencies and damping ratios in the frequency band $0 - 500$ Hz: (1) $f_1 = 23.8$ Hz, $\zeta_1 = 0.33\,\%$, (2) $f_2 = 148.1$ Hz, $\zeta_2 = 0.052\,\%$, and (3) $f_3 = 414.4$ Hz, $\zeta_3 = 0.024\,\%$. The natural frequencies are not close to each other so no significant mode mixing in the EMD should occur unless there is a prominent difference in amplitudes. The damping ratios are relatively small, being less than 0.1 % for higher modes. This fact justified the use of the ECL benchmark in the studies about NNMs [15, 67] in which the damping is not considered but the conservative system can be still adequately studied.

The estimation of the complex non-linear modes is demonstrated on the free decay responses which were measured by applying a short impact to node 9. All three accelerometers simultaneously acquired the

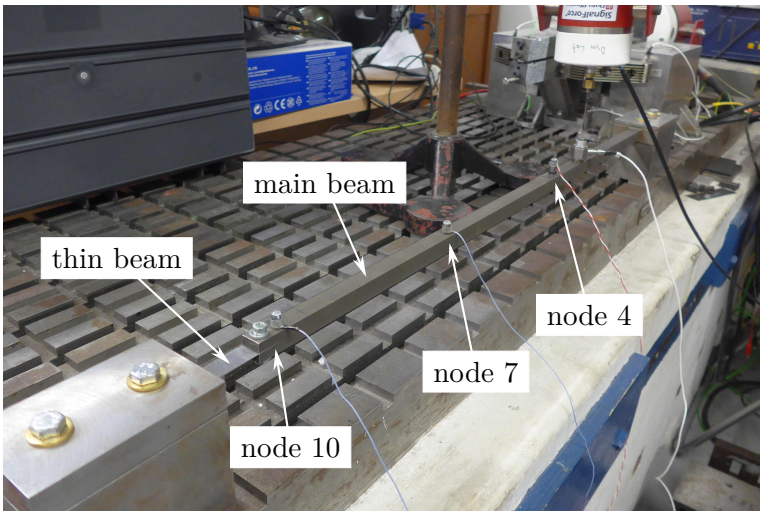


Figure 16: Experimental set-up of the ECL benchmark used for the demonstration of non-linear modes estimation from a free decay. The shaker shown in the figure was not attached during the measurement.

response in nodes 4,7 and 10. The processing will be shown in detail for the responses of node 4 and 10 shown in Fig. 17. These responses have a multi-component character so the IF and IA cannot be directly

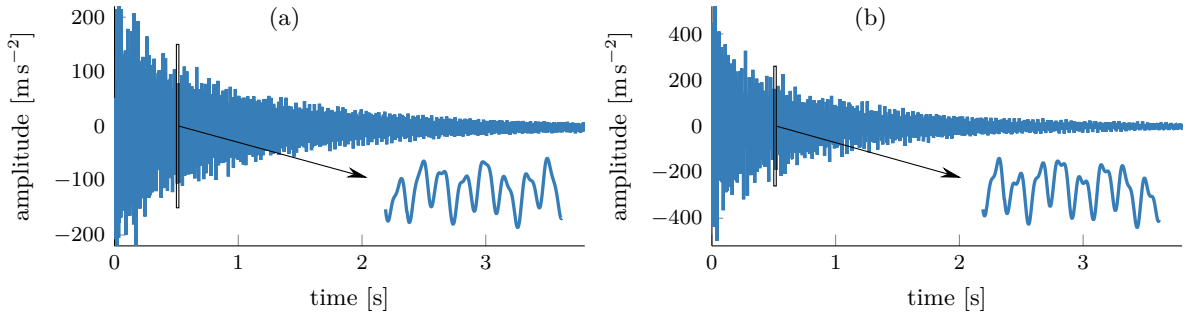


Figure 17: The measured free decay acceleration of the ECL benchmark: (a) node 4 and (b) node 10

estimated. Therefore, the EMD must be applied to obtain the IMFs. Since the acceleration was measured, the responses have been integrated twice to obtain the required form of data. It should be noted that a trend in the data usually appears after the integration. This trend can be removed by standard de-trending algorithms or it can be left in the data, because the EMD will remove it automatically as well.

The EMD was not initially able to estimate clear modes that would be close to nominal linear modes due to mode mixing problems which occurred due to the prominent difference in amplitudes. However, by applying the masking signal approach repeatedly (for each IMFs a different masking signal was used), it was possible to separate the three intrinsic mode functions shown in Fig. 18. These IMFs correspond to the first three non-linear modes of the structure. It can be seen that the IMFs look like individual resonant decay responses. Compared to the IMFs of a cantilever beam in Fig. 14 they are not so noisy. This is caused by the fact that not so many modes were excited in this experiment. In fact, there were only a few spurious IMFs which did not seem to have any relation to the non-linear modes and which had an order of magnitude lower amplitude. Most of them seemed to be a consequence of the data processing so they were not shown here. Although the IMFs appear to be sufficiently smooth, some end-effects can be seen at the beginning and the end of the signals. These regions are therefore excluded from the subsequent analyses.

The IF and IA have been estimated by the ZC method. Consequently, the backbones were calculated

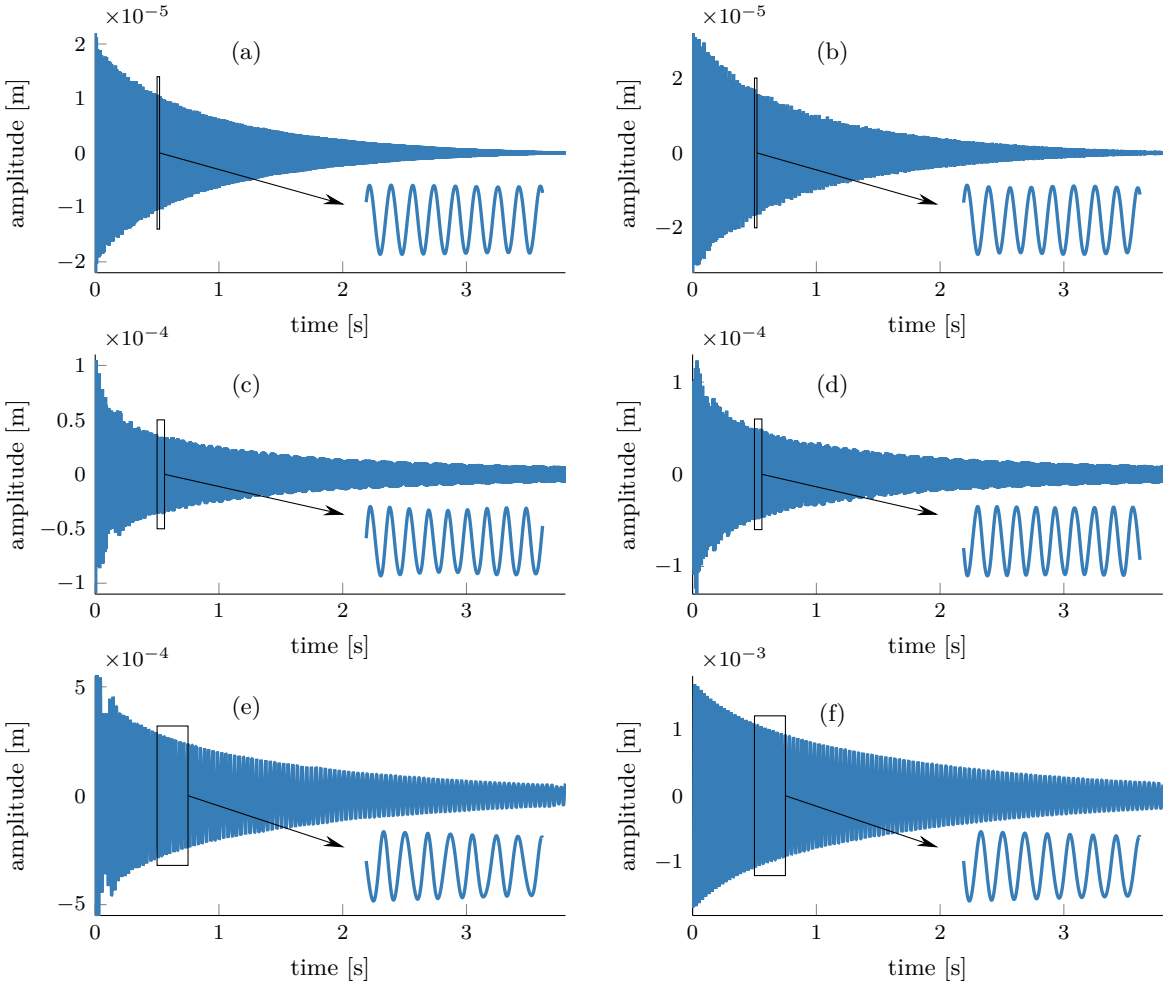


Figure 18: Intrinsic mode functions extracted from free decays of the ECL benchmark: (a) 3rd mode, node 4, (b) 3rd mode, node 10, (c) 2nd mode, node 4, (d) 2nd mode, node 4, (e) 1st mode, node 4, and (f) 1st mode, node 10

and the damping assessed by the logarithm of the amplitude as described in section 2.1.3. The results are shown in Fig. 19. From the backbones, it is immediately obvious that the system is non-linear and that it exhibits the hardening type of non-linearity. The hardening behaviour can be observed in all three investigated modes. The frequency shift is dominant for the first mode (over 10 Hz) and smaller for the second and third mode. It can be also noticed that the frequencies for very low amplitudes (presumably linear natural frequencies) are not identical to the frequency of the main beam without the non-linearity. The first frequency is slightly higher whereas the other two are slightly lower. It was found that this phenomenon is caused by the thin beam which, besides introducing the non-linearity, adds the linear stiffness that causes the shift of the frequencies.

No significant non-linearity in damping can be observed from the logarithm of the amplitude in Fig. 19. Therefore, the linear damping ratios can be estimated by the line fitting which yields $\zeta_1 = 0.3415\,\%$, $\zeta_2 = 0.0539\,\%$ and $\zeta_3 = 0.0396\,\%$. The estimated values are slightly higher than the values obtained by the linear modal analysis. The small discrepancies do not have to be solely caused by the presence of the thin beam. They can also be a consequence of different estimation methods.

It should be also mentioned that the backbone in Fig. 19(b) for node 7 is not estimated for the frequency higher than 150 Hz. Likewise, the factor $d_2^7(t)$ in Fig. 19(e) is not available for the time lower than 0.7 s. These missing parts of the results are a consequence of the end effects that occurred in the EMD. It is

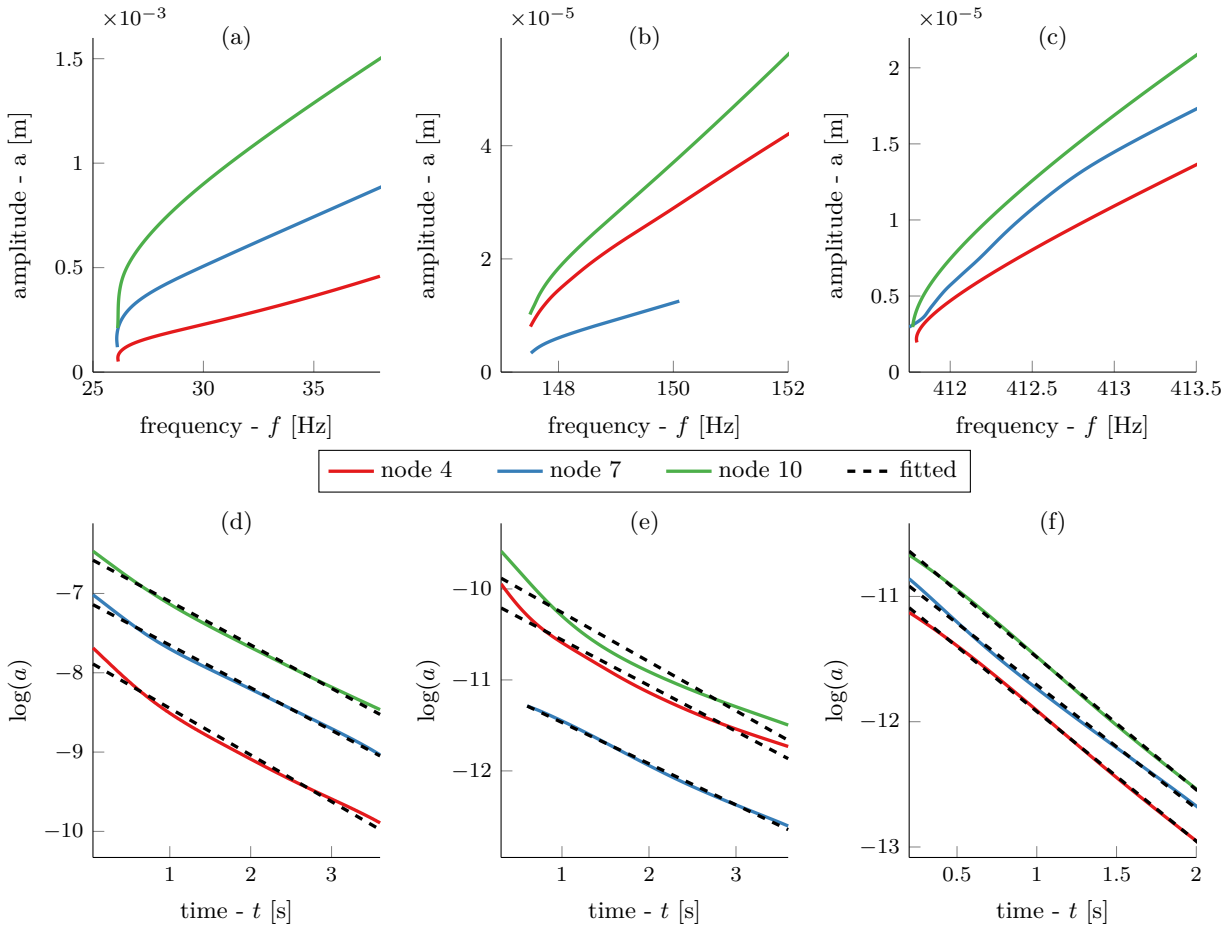


Figure 19: Estimated non-linear modes of the ECL benchmark: (a)-(c) the backbones of the first three modes and (d)-(f) the logarithms of the vibration amplitude of the first three modes

possible that the second mode in node 7 is influenced by the end-effects more than the other results, because node 7 lies close to the node of vibration (zero value of mode shape) of the second mode. Therefore, the data acquired are more likely to be corrupted by measured noise and processing errors.

The mode shapes estimated according to section 2.1.3 as a function of time are shown in Fig. 20. It is clear that the character of the mode shapes estimated for the non-linear system is the same as the well-known linear mode shapes of a cantilever beam. This was expected because the estimated non-linear modes are the continuation of their linear companions.

In order to illustrate the change of the mode shapes due to the non-linearity, the first two modes shapes are shown in Fig. 21 again. The third mode is not included because it did not show any significant change. It can be seen that the mode shapes change with the frequency (and therefore amplitude) of vibration. The normalised values of the first mode increase for the higher frequency whereas the normalised amplitude of the second mode decreases. This is consistent with the simulated CNMs of the beam with a geometric non-linearity seen in Fig. 12(c) and Fig. 12(d). The estimated modes shown not only confirm the presence of the cubic hardening but also demonstrate the ability of the HHT to obtain multiple non-linear modes from a single measurement.

*Summary of the application to experimental data*

The estimation of several non-linear modes has been demonstrated using experimental free decay responses obtained from the ECL benchmark. It was possible to recover three non-linear modes, two of which

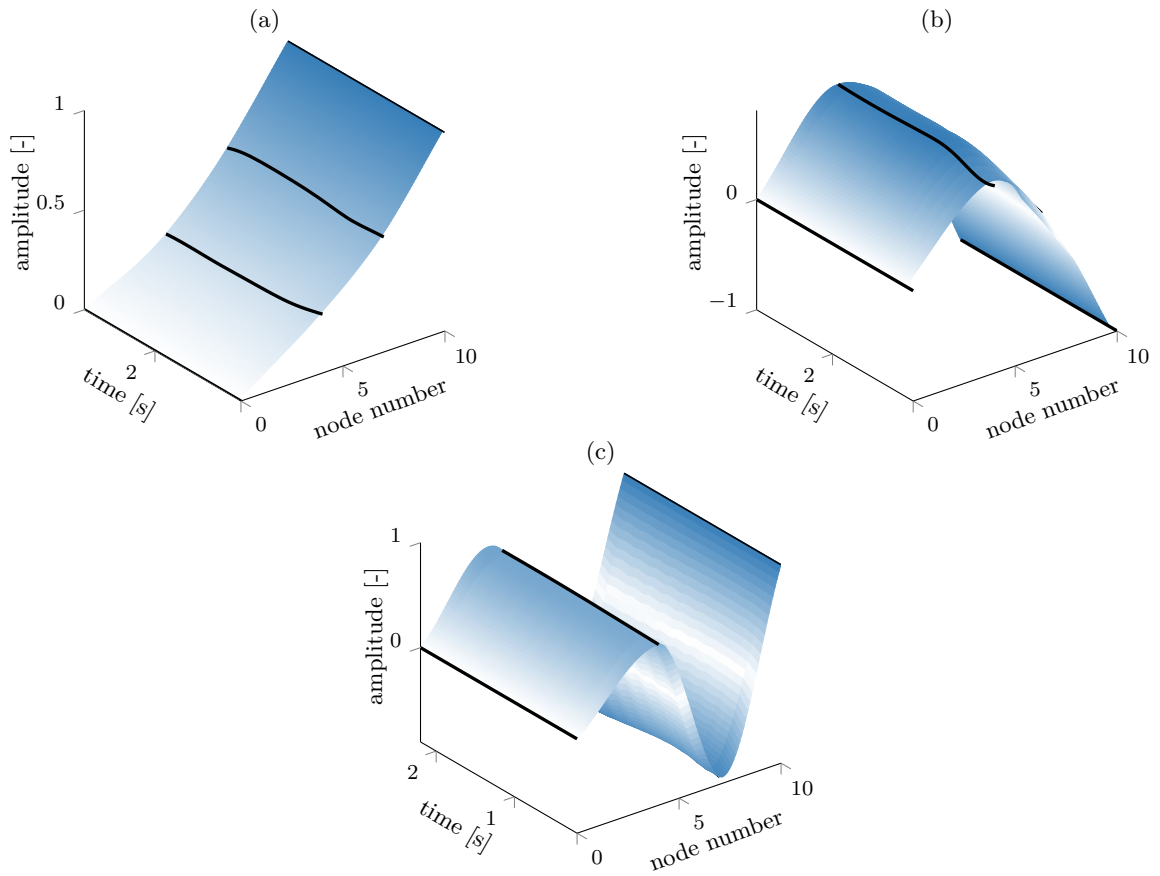


Figure 20: The estimated mode shapes of the ECL benchmark as a function of time: (a) 1st mode, (b) 2nd mode, and (c) 3rd mode

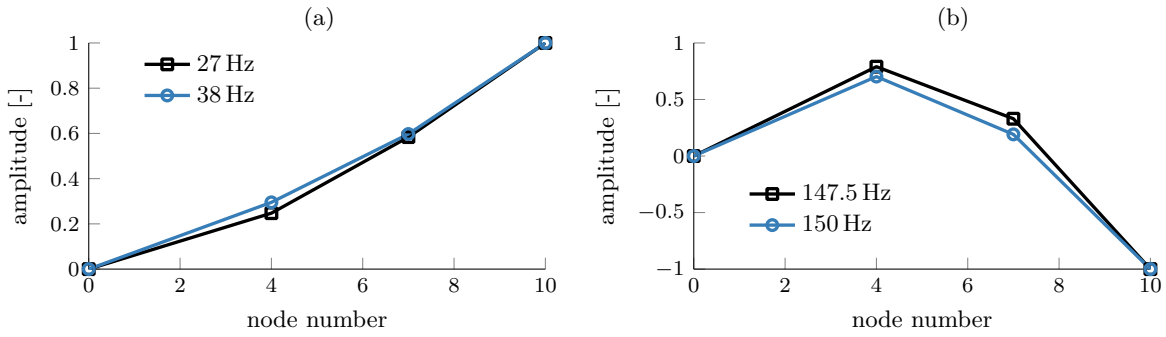


Figure 21: Estimated modes shapes of the ECL benchmark: (a) 1st mode and (b) 2nd mode. These estimated mode shapes are very similar to the mode shapes of the simulated cantilever beam shown in Fig. 12.

show a noticeable change of the mode shape with vibration amplitude. The first two modes shapes qualitatively correspond to the modes of simulated cantilever beam with stiffness non-linearity and also correspond to available literature. It should be emphasised that all these modes have been estimated from a single data set which was measured using a simple impact excitation. Based on this experimental demonstration it can be concluded that the non-linear modes can be successfully estimated from an experimentally measured free decay response and can be used for detection and characterisation. Due to the findings in section 3 it cannot

be expected that these modes correspond accurately to the correct complex non-linear modes which could be used to quantify the system's parameters.

## 5. Discussion

The objective of this paper was to show how the Hilbert-Huang transform can be used to estimate the complex non-linear modes of mechanical systems and assess their accuracy. It was hypothesised that the HHT should be able to estimate the CNMs due to a number of similarities between the IMFs and ROM. The link among these methods has been established by the slow-flow dynamics and supported by a variety of numerical cases and parametric studies in section 3. Unfortunately, it was found that this link holds only approximately, i.e. the HHT can recover qualitatively correct CNMs which are suitable for detection and characterisation of non-linearities, but they cannot be used to quantify the system's parameters.

A similar relation was already utilised in a number of papers [31, 54, 74, 75] where the HHT was used for non-linear system identification in a non-linear normal mode (NNM) framework. In these studies, it was intuitively assumed that the IMFs should compose some approximation of the responses of individual NNMs. Subsequently, the estimated IF and IA should correspond to the computed backbones. However, the NNMs are not defined for non-conservative system, so their use for non-linear system identification of dissipative systems might be sometimes complicated, at least ideologically. The use of CNMs appears to be preferable since the applicability to non-conservative systems can be guaranteed.

The HHT does not have a rigid mathematical background and therefore no exact mathematical proof of the concepts discussed in this paper can be given, but the physics-based foundation was already established [33, 48]. This was achieved by showing the correspondence of the IMFs and slow-flow dynamics derived by the CxA. This relation has been used throughout this study to investigate the accuracy of the CNMs obtained by the HHT. The CxA is an analytical method and its applicability is therefore limited to small academic systems with simple non-linearities. In contrast, the CNMs can be numerically computed for large industrial structures with complex non-linearities [19–22] while no analytical solution is possible. Therefore, effectively replacing the CxA with the ROM may extend the applicability to a broader range of non-linear systems with complex non-linearities. This means that the gap in using non-linear modal analysis between the academic studies and industrial application has been slightly reduced.

In full accordance with the fundamental restriction of the ROM, i.e. it does not take into account more than one mode which automatically excludes any modal interactions, the response is predicted accurately in the close proximity of a non-linear mode. This accuracy was shown for the resonant decay responses in [23]. In addition, the accuracy was demonstrated for near resonance forcing, provided by a slow sweep excitation, in [23, 50]. These cases are trivial from the point of view of the presented topic, because the EMD, a key and unique concept of the HHT, does not have to be applied so they were not presented in the paper.

In [30, 33, 48], it was concluded that the CxA led to the satisfactory approximation of the response. A similar degree of approximation has been observed for the ROM derived by the CNMs in this paper. The approximation of the total response was already theorised in [23] where it was stated that by simply superimposing the ROM responses of several modes, the total response could be obtained. Although this paper did not target this in particular detail, it partly addressed this issue too. It has been found that the response of the ROM approximates the IMFs and since the superposition of the IMFs always gives the total response (guaranteed by Eq. (1)), it follows that also the superposition of the ROM responses leads to the total response. Therefore, the theoretical claim from [23] seems validated, but the total response is not obtained exactly, but only approximately. This is also in line with [63] which showed that the concept of invariant manifold also approximatively leads to the total response. Since CNMs trace trajectories on the manifolds, their superposition should also lead to the approximation of the total response.

It was shown that even for noise-free free decay responses, the match of the ROM response and IMFs is not exact. Furthermore, since the HHT is primarily used for the processing of experimental data, the errors originating in experimental setting imperfections, measured noise, and data processing uncertainty might further increase the margin of this approximation. Therefore, it cannot be concluded that the CNMs and related ROM provide mathematical framework for the empirical HHT. This means that the HHT cannot be used for quantification the quantification of system's parameters using CNMs.

The range of validity and applicability of the identification of CNMs using the HHT is given by the limitations of the methods involved. Several important limitations are introduced by the HHT, especially by the EMD. The most concerning one is the mode mixing problem. However, it was described in section 2.1.1 that by applying a simple procedure, the frequency splitting capabilities can be investigated before applying the EMD. This has been demonstrated in the second parametric study where the region in which the EMD can accidentally extract spurious IMFs was not considered. The mode mixing may also be overcome by increasing the number of shifting iterations [36] or by applying some of the advanced EMD schemes, such as a masking signal [48, 51], ensemble empirical mode decomposition (EEMD) [52], empirical mode decomposition using unconstrained optimisation [53] or wavelet-bounded empirical mode decomposition (WBEMD) [54]. It must be however emphasised that using one of the advanced EMD schemes does not mean that the relation between the IMFs and ROM would be improved, and therefore more accurate CNMs could be estimated. In the region where the EMD does not suffer from the mode mixing problem (as described in section 2.1.1), any of the advanced EMD schemes should give the same IMFs. Therefore, the basic EMD used in this paper does not present a limitation with regards to the assessment of the accuracy of the estimated complex non-linear modes presented in section 3.

One more problem associated with the HHT can be troublesome in practical situations. The EMD yields, by definition, symmetric IMFs so when applied to systems with asymmetric restoring forces it can lead to physically incorrect conclusions. Moreover, even if the resonant decay response of a system with asymmetric non-linearity is measured, the Hilbert transform or any of its alternatives cannot estimate the forces correctly (the Freevib algorithm cannot be used in a presence of asymmetric restoring forces [59]). The analysis of the systems with asymmetric non-linearities, including gaps, pre-stress effects and piece-wise linear stiffness, has just recently been allowed by the Hilbert vibration decomposition (HVD) [76]. However, the HVD is difficult to used due to a number of sophisticated signal processing techniques needed. A new method which is based on the zero-crossing, has been recently proposed in [77]. The developed method as well as the HVD provide equivalent results which characterise the non-linear behaviour in terms of congruent functions. Whether or not the congruent functions relate, at least approximately, to the CNMs is not clear because the congruent functions, which are a direct consequence of the selected signal processing [44], cannot be analytically or numerically computed.

A key limitation given by the ROM derived from the CNMs is its incapability to deal with internal resonances. Therefore, internal resonances have been excluded from the consideration in this paper. It can be, however, stated that the identification of the CNMs using the HHT is not guaranteed in the presence of internal resonances, because the key link cannot be found. It is quite possible, that this limitation of the ROM will be removed in the future. The concepts of the CNMs and associated ROM have just recently been developed and are still establishing their place in the field of non-linear dynamics. It has been already suggested that the future development of the ROM should address the cases where modal interactions do exist [23]. When and if such extended ROM is developed, it is possible that the accuracy and a range of applicability of the argued relation between the IMFs and ROM will extend too. It can be only hypothesised that the ROM which includes several non-linear modes would lead to the IMFs exactly.

However, even if the ROM could describe the internal resonances, it is unclear how the HHT should be used to study them. Due to its definition, the HHT cannot extract dependencies between the IMFs (the IMFs are practically orthogonal to each other). Therefore, while the traditional HHT can be used to detect internal resonances [34, 35, 54, 75], it may not be able to provide any further details about them. However, an extension of the HHT, called the Holo-Hilbert spectral analysis (HHSA) method [78], has been recently proposed. Theoretically, it should allow to recover cross-scale coupling between the IMFs so it may perhaps be possible to study internal resonances using this method. It has never been applied in structural dynamics so its practical feasibility is yet to be determined.

It should be also noted that the relation between the IMFs and ROM is exact for linear systems (as shown, for example, in Fig. 6) so the HHT can be also used for linear modal analysis as in [38, 39]. However, since the system is linear, it is better to use other techniques for linear modal analysis, thereby avoiding potential numerical imperfections of the HHT. For non-linear systems, the relation between the IMFs and ROM theoretically provides a base for non-linear experimental modal analysis as proposed in [79]. However, the quantification of non-linear behaviour would work well only for the cases where the relation of the HHT

estimated the CNMs accurately, i.e. for resonant free decays and nearly resonant forcing. The accuracy of the method proposed in [79] is limited for general initial conditions, because the relation between the IMFs and ROM found in this paper is only approximative.

From the findings presented in this paper, it would seem that the Hilbert-Huang transform loses its importance with regards to non-linear system identification in a non-linear modal analysis framework. However, it should be emphasised that the presented approach is a straightforward evaluation of the possible relation using the methods that are available in the literature at the moment. It is believed that further research, such as a development of a mode participation factor that would account for the presence of multiple modes in section 2.1.3, could be conducted to allow the use of the HHT as a universal, non-parametric means of non-linear modal analysis.

## 6. Conclusion

The objective of this paper has been to present the identification of the complex non-linear modes using the Hilbert-Huang transform from free decay responses and to systematically assess their accuracy. The conducted numerical studies led to an important conclusion - the Hilbert-Huang transform is able to estimate the complex non-linear modes that are suitable for detection and characterisation of non-linear behaviour, but not for its quantification. The estimation of several non-linear modes has also been demonstrated using experimental data obtained from the ECL benchmark. It was possible to extract three non-linear modes, two of which showed a noticeable change of the mode shape with vibration amplitude. The first two mode shapes qualitatively corresponded to the modes of the simulated cantilever beam with stiffness non-linearity and also to available literature. The findings presented in this paper mean that the ability of the Hilbert-Huang transform to quantify a structural non-linearity using non-linear modes is very limited although detection and characterisation in a non-parametric manner are possible.

## Acknowledgements

The authors are grateful to Rolls-Royce plc for providing the financial support for this project and for giving permission to publish this work. This work is part of a Collaborative R&T Project "SAGE 3 WP4 Nonlinear Systems" supported by the CleanSky Joint Undertaking and carried out by Rolls-Royce plc and Imperial College London.

## References

[1] D. J. Ewins, Modal Testing: Theory, Practice and Application, Research studies press Ltd, 2000.
[2] K. Worden, G. R. Tomlinson, Nonlinearity in Structural Dynamics: Detection, Identification and Modelling, Institute of Physics Publishing, Bristol and Philadelphia, 2001.
[3] K. Worden, P. L. Green, A machine learning approach to nonlinear modal analysis, Mechanical Systems and Signal Processing 84, Part B (2017) 34 – 53. doi:10.1016/j.ymssp.2016.04.029.
[4] L. Renson, G. Kerschen, B. Cochelin, Numerical computation of nonlinear normal modes in mechanical engineering, Journal of Sound and Vibration 364. doi:10.1016/j.jsv.2015.09.033.
[5] J.-P. Noël, L. Renson, C. Grappasonni, G. Kerschen, Identification of nonlinear normal modes of engineering structures under broadband forcing, Mechanical Systems and Signal Processing 74 (2016) 95–110. doi:10.1016/j.ymssp.2015.04.016.
[6] K. J. Moore, A. Mojahed, M. Kurt, M. Eriten, D. M. McFarland, L. A. Bergman, A. F. Vakakis, Advanced nonlinear system identification for modal interactions in nonlinear structures: A review, in: I. V. Andrianov, A. I. Manevich, Y. V. Mikhlin, O. V. Gendelman (Eds.), Problems of Nonlinear Mechanics and Physics of Materials, Springer International Publishing, 2019, pp. 101–118. doi:10.1007/978-3-319-92234-8_7.
[7] G. Kerschen, M. Peeters, J.-C. Golinval, A. F. Vakakis, Nonlinear normal modes, Part I: A useful framework for the structural dynamicist, Mechanical Systems and Signal Processing 23 (1) (2009) 170–194. doi:10.1016/j.ymssp.2008.04.002.
[8] Y. V. Mikhlin, K. V. Avramov, Nonlinears normal modes for vibrating mechanical systems. Review of theoretical developments, Applied Mechanics Reviews 63 (6) (2011) 060802–21. doi:10.1115/1.4003825.
[9] A. F. Vakakis, Non-linear normal modes (NNMs) and their applications in vibration theory: An overview, Mechanical Systems and Signal Processing 11 (1) (1997) 3–22. doi:10.1006/mssp.1996.9999.
[10] A. F. Vakakis, Normal Modes and Localization in Nonlinear Systems, Springer, 2001. doi:10.1007/978-94-017-2452-4.

[11] C. Pierre, D. Jiang, S. Shaw, Nonlinear normal modes and their application in structural dynamics, Mathematical Problems in Engineering 2006 (2006) 1–15. doi:10.1155/MPE/2006/10847.
[12] K. V. Avramov, Y. V. Mikhlin, Review of applications of nonlinear normal modes for vibrating mechanical systems, Applied Mechanics Reviews 65 (2) (2013) 020801–20. doi:10.1115/1.4023533.
[13] R. M. Rosenberg, On nonlinear vibrations of systems with many degrees of freedom, Advances in Applied Mechanics 9 (1966) 155–242. doi:10.1016/S0065-2156(08)70008-5.
[14] M. Peeters, G. Kerschen, J.-C. Golinval, Dynamic testing of nonlinear vibrating structures using nonlinear normal modes, Journal of Sound and Vibration 330 (3) (2011) 486–509. doi:10.1016/j.jsv.2010.08.028.
[15] M. Peeters, G. Kerschen, J.-C. Golinval, Modal testing of nonlinear vibrating structures based on nonlinear normal modes: Experimental demonstration, Mechanical Systems and Signal Processing 25 (4) (2011) 1227–1247. doi:10.1016/j.ymssp.2010.11.006.
[16] M. Peeters, R. Viguié, G. Sérandour, G. Kerschen, J.-C. Golinval, Nonlinear normal modes, Part II: Toward a practical computation using numerical continuation techniques, Mechanical Systems and Signal Processing 23 (1) (2009) 195–216. doi:10.1016/j.ymssp.2008.04.003.
[17] D. A. Ehrhardt, M. S. Allen, Measurement of nonlinear normal modes using multi-harmonic stepped force appropriation and free decay, Mechanical Systems and Signal Processing 7677 (2016) 612–633. doi:10.1016/j.ymssp.2016.02.063.
[18] S. W. Shaw, C. Pierre, Normal modes for non-linear vibratory systems, Journal of Sound and Vibration 164 (1) (1993) 85–124. doi:10.1006/jsvi.1993.1198.
[19] D. Laxalde, F. Thouverez, Complex non-linear modal analysis for mechanical systems: Application to turbomachinery bladings with friction interfaces, Journal of Sound and Vibration 322 (4-5) (2009) 1009–1025. doi:10.1016/j.jsv.2008.11.044.
[20] M. Krack, L. Panning-Von Scheidt, J. Wallaschek, A method for nonlinear modal analysis and synthesis: Application to harmonically forced and self-excited mechanical systems, Journal of Sound and Vibration 332 (25) (2013) 6798–6814. doi:10.1016/j.jsv.2013.08.009.
[21] M. Krack, L. Salles, F. Thouverez, Vibration prediction of bladed disks coupled by friction joints, Archives of Computational Methods in Engineering (2016) 1–48doi:10.1007/s11831-016-9183-2.
[22] D. Laxalde, L. Salles, L. Blanc, F. Thouverez, Non-linear modal analysis for bladed disks with friction contact interfaces, in: ASME Turbo Expo: Power for Land, Sea, and Air, Volume 5: Structures and Dynamics, Parts A and B, Berlin, Germany, 2008, pp. 457–467. doi:10.1115/GT2008-50860.
[23] M. Krack, L. Panning-Von Scheidt, J. Wallaschek, On the computation of the slow dynamics of nonlinear modes of mechanical systems, Mechanical Systems and Signal Processing 42 (1-2) (2014) 71–87. doi:10.1016/j.ymssp.2013.08.031.
[24] G. Kerschen, K. Worden, A. F. Vakakis, J.-C. Golinval, Past, present and future of nonlinear system identification in structural dynamics, Mechanical Systems and Signal Processing 20 (3) (2006) 505–592. doi:10.1016/j.ymssp.2005.04.008.
[25] S. F. Masri, T. K. Caughey, A nonparametric identification technique for nonlinear dynamic problems, Journal of Applied Mechanics 46 (2) (1979) 433–447. doi:10.1115/1.3424568.
[26] S. A. Billings, Nonlinear System Identification: NARMAX Methods in Time, Frequency, and Spatio-Temporal Domains, Wiley-Blackwell, 2013.
[27] V. Ondra, R. Riethmueller, M. R. W. Brake, C. W. Schwingshackl, P. M. Polunin, S. W. Shaw, Comparison of nonlinear system identification methods for free decay measurements with application to MEMS devices, in: E. Wee Sit, C. Walber, P. Walter, S. Seidlitz (Eds.), Sensors and Instrumentation, Volume 5. Conference Proceedings of the Society for Experimental Mechanics Series, Los Angeles, California, USA, 2017, pp. 29–46. doi:10.1007/978-3-319-54987-3_5.
[28] P. Flandrin, Time-frequency/Time-scale Analysis, Academic Press, 1999.
[29] J. R. Wright, J. E. Cooper, M. J. Desforges, Normal-mode force appropriation - theory and application, Mechanical Systems and Signal Processing 13 (2) (1999) 217 – 240. doi:10.1006/mssp.1998.1214.
[30] Y. S. Lee, S. Tsakirtzis, A. F. Vakakis, L. A. Bergman, D. M. McFarland, A time-domain nonlinear system identification method based on multiscale dynamic partitions, Meccanica 46 (4) (2011) 625–649. doi:10.1007/s11012-010-9327-7.
[31] P. F. Pai, Time–frequency characterization of nonlinear normal modes and challenges in nonlinearity identification of dynamical systems, Mechanical Systems and Signal Processing 25 (7) (2011) 2358–2374. doi:10.1016/j.ymssp.2011.02.013.
[32] M. Feldman, Hilbert Transform Application in Mechanical Vibration, John Wiley & Sons Ltd, 2011. doi:10.1002/9781119991656.
[33] G. Kerschen, A. F. Vakakis, Y. S. Lee, M. D. Mcfarland, L. A. Bergman, Toward a fundamental understanding of the Hilbert-Huang transform in nonlinear structural dynamics, Journal of Vibration and Control 14 (1-2) (2008) 77–105. doi:10.1177/1077546307079381.
[34] M. Kurt, M. Eriten, M. D. Mcfarland, L. A. Bergman, A. F. Vakakis, Strongly nonlinear beats in the dynamics of an elastic system with a strong local stiffness nonlinearity: Analysis and identification, Journal of Sound and Vibration 333 (7) (2014) 2054–2072. doi:10.1016/j.jsv.2013.11.021.
[35] M. Kurt, H. Chen, Y. S. Lee, D. M. McFarland, L. A. Bergman, A. F. Vakakis, Nonlinear system identification of the dynamics of a vibro-impact beam: numerical results, Archive of Applied Mechanics 82 (10) (2012) 1461–1479. doi:10.1007/s00419-012-0678-5.
[36] N. E. Huang, Z. Shen, S. R. Long, M. C. Wu, H. H. Shih, Q. Zheng, N.-C. Yen, C. C. Tung, H. H. Liu, The empirical mode decomposition and the Hilbert spectrum for nonlinear and non-stationary time series analysis, Proceedings of the Royal Society of London A: Mathematical, Physical and Engineering Sciences 454 (1971) (1998) 903–995. doi:10.1098/rspa.1998.0193.

[37] N. E. Huang, Z. Wu, S. R. Long, K. C. Arnold, X. Chen, K. Blank, On instantaneous frequency, Advances in Adaptive Data Analysis 1 (2) (2009) 177–229. doi:10.1142/S1793536909000096.
[38] J. N. Yang, Y. Lei, S. Pan, N. E. Huang, System identification of linear structures based on Hilbert-Huang spectral analysis. Part 1: normal modes, Earthquake Engineering & Structural Dynamics 32 (9) (2003) 1443–1467. doi:10.1002/eqe.287.
[39] J. N. Yang, Y. Lei, S. Pan, N. E. Huang, System identification of linear structures based on Hilbert-Huang spectral analysis. Part 2: Complex modes, Earthquake Engineering & Structural Dynamics 32 (10) (2003) 1533–1554. doi:10.1002/eqe.288.
[40] S. Qin, Q. Wang, J. Kang, Output-only modal analysis based on improved empirical mode decomposition method, Advances in Materials Science and Engineering 2015 (2015) 1–12. doi:10.1155/2015/945862.
[41] B. Chen, S. Zhao, P. Li, Application of Hilbert-Huang transform in structural health monitoring: a state-of-the-art review, Mathematical Problems in Engineering 2014 (2014) 1–22. doi:10.1155/2014/317954.
[42] P. F. Pai, Time-frequency analysis for parametric and non-parametric identification of nonlinear dynamical systems, Mechanical Systems and Signal Processing 36 (2) (2013) 332–353. doi:10.1016/j.ymssp.2012.12.002.
[43] P. F. Pai, B.-A. Nguyen, M. J. Sundaresan, Nonlinearity identification by time-domain-only signal processing, International Journal of Non-Linear Mechanics 54 (2013) 85–98. doi:10.1016/j.ijnonlinmec.2013.04.002.
[44] M. Feldman, Hilbert transform in vibration analysis, Mechanical Systems and Signal Processing 25 (3) (2011) 735–802. doi:10.1016/j.ymssp.2010.07.018.
[45] S. Braun, M. Feldman, Decomposition of non-stationary signals into varying time scales: Some aspects of the EMD and HVD methods, Mechanical Systems and Signal Processing 25 (7) (2011) 2608–2630. doi:10.1016/j.ymssp.2011.04.005.
[46] P. F. Pai, A. N. Palazotto, HHT-based nonlinear signal processing method for parametric and non-parametric identification of dynamical systems, International Journal of Mechanical Sciences 50 (12) (2008) 1619–1635. doi:10.1016/j.ijmecsci.2008.10.001.
[47] S. Tsakirtzis, Y. S. Lee, A. F. Vakakis, L. A. Bergman, M. D. Mcfarland, Modelling of nonlinear modal interactions in the transient dynamics of an elastic rod with an essentially nonlinear attachment, Communications in Nonlinear Science and Numerical Simulation 15 (9) (2010) 2617–2633. doi:10.1016/j.cnsns.2009.10.014.
[48] Y. S. Lee, S. Tsakirtzis, A. F. Vakakis, L. A. Bergman, M. D. McFarland, Physics-based foundation for empirical mode decomposition, AIAA Journal 47 (12) (2009) 2938–2963. doi:10.2514/1.43207.
[49] G. Rilling, P. Flandrin, One or two frequencies? The empirical mode decomposition answers, IEEE Transactions on Signal Processing 56 (1) (2008) 85–95. doi:10.1109/TSP.2007.906771.
[50] V. Ondra, Non-linear System Identification in Structural Dynamics: Advances in Characterisation of Non-linearities and Non-linear Modal Analysis, PhD Thesis, Imperial College London (2017).
[51] R. Deering, J. F. Kaiser, The use of a masking signal to improve empirical mode decomposition, Proceedings of IEEE International Conference on Acoustics, Speech and Signal Processing IV (2005) 485–488. doi:10.1109/ICASSP.2005.1416051.
[52] Z. Wu, N. E. Huang, Ensemble Empirical Mode Decomposition: a noise-assisted data analysis method, Advances in Adaptive Data Analysis 1 (1) (2009) 1–41. doi:10.1142/S1793536909000047.
[53] M. Colominas, G. Schlotthauer, M. E. Torres, An unconstrained optimization approach to empirical mode decomposition, Digital Signal Processing 40 (2015) 164–175. doi:10.1016/j.dsp.2015.02.013.
[54] K. J. Moore, M. Kurt, M. Eriten, D. M. McFarland, L. A. Bergman, A. F. Vakakis, Wavelet-bounded empirical mode decomposition for vibro-impact analysis, Nonlinear Dynamics 93 (3) (2018) 1559–1577. doi:10.1007/s11071-018-4276-0.
[55] S. L. Marple, Computing the discrete-time analytic signal via FFT, IEEE Transactions on Signal Processing 47 (9) (1999) 2600–2603. doi:10.1109/78.782222.
[56] V. Ondra, I. A. Sever, C. W. Schwingshackl, A method for detection and characterisation of structural non-linearities using the Hilbert transform and neural networks, Mechanical Systems and Signal Processing 83 (2017) 210–227. doi:10.1016/j.ymssp.2016.06.008.
[57] F. Salzenstein, A.-O. Boudraa, J.-C. Cexus, Generalized higher-order nonlinear energy operators, Journal of Optical Society of America A 24 (12) (2007) 3717–3727. doi:10.1364/JOSAA.24.003717.
[58] J. M. Londoño, S. A. Neild, J. E. Cooper, Identification of backbone curves of nonlinear systems from resonance decay responses, Journal of Sound and Vibration 348 (2015) 224–238. doi:10.1016/j.jsv.2015.03.015.
[59] M. Feldman, Non-linear system vibration analysis using Hilbert transform–I. Free vibration analysis method 'Freevib', Mechanical Systems and Signal Processing 8 (2) (1994) 119–127. doi:10.1006/mssp.1994.1011.
[60] M. Feldman, Non-linear system vibration analysis using Hilbert transform–II. Forced vibration analysis method 'Forcevib', Mechanical Systems and Signal Processing 8 (3) (1994) 309–318. doi:10.1006/mssp.1994.1023.
[61] T. M. Cameron, J. H. Griffin, An alternating frequency/time domain method for calculating the steady-state response of nonlinear dynamic systems, Journal of Applied Mechanics 56 (1) (1989) 149–154. doi:10.1115/1.3176036.
[62] T. Detroux, L. Renson, L. Masset, G. Kerschen, The harmonic balance method for bifurcation analysis of large-scale nonlinear mechanical systems, Computer Methods in Applied Mechanics and Engineering 296 (2015) 18–38. doi:10.1016/j.cma.2015.07.017.
[63] E. Pesheck, N. Boivin, C. Pierre, S. W. Shaw, Nonlinear modal analysis of structural systems using multi-mode invariant manifolds, Nonlinear Dynamics 25 (1) (2001) 183–205. doi:10.1023/A:1012910918498.
[64] T. L. Hill, P. L. Green, A. Cammarano, S. A. Neild, Fast Bayesian identification of a class of elastic weakly nonlinear systems using backbone curves, Journal of Sound and Vibration 360 (2016) 156–170. doi:10.1016/j.jsv.2015.09.007.
[65] D. Göge, M. Sinapius, U. Füllekrug, M. Link, Detection and description of non-linear phenomena in experimental modal analysis via linearity plots, International Journal of Non-Linear Mechanics 40 (1) (2005) 27–48. doi:10.1016/j.ijnonlinmec.2004.05.011.
[66] F. Thouverez, Presentation of the ECL benchmark, Mechanical Systems and Signal Processing 17 (1) (2003) 195–202.

doi:10.1006/mssp.2002.1560.
[67] M. Peeters, Theoretical and Experimental Modal Analysis of Nonlinear Vibrating Structures using Nonlinear Normal Modes, PhD Thesis, University of Liege (2010).
[68] N. E. Huang, Z. Shen, S. R. Long, A new view of nonlinear water waves: The Hilbert spectrum, Annual Review of Fluid Mechanics 31 (1) (1999) 417–457. doi:10.1146/annurev.fluid.31.1.417.
[69] G. Kerschen, V. Lenaerts, J.-C. Golinval, Identification of a continuous structure with a geometrical non-linearity. Part I: Conditioned reverse path method, Journal of Sound and Vibration 262 (4) (2003) 889–906. doi:10.1016/S0022-460X(02)01151-3.
[70] V. Lenaerts, G. Kerschen, J.-C. Golinval, Identification of a continuous structure with a geometrical non-linearity. Part II: Proper orthogonal decomposition, Journal of Sound and Vibration 262 (4) (2003) 907–919. doi:10.1016/S0022-460X(02)01132-X.
[71] P. Argoul, T.-P. Le, Instantaneous indicators of structural behaviour based on the continuous Cauchy wavelet analysis, Mechanical Systems and Signal Processing 17 (1) (2003) 243–250. doi:10.1006/mssp.2002.1557.
[72] S. Meyer, M. Link, Modelling and updating of local non-linearities using frequency response residuals, Mechanical Systems and Signal Processing 17 (1) (2003) 219–226. doi:10.1006/mssp.2002.1563.
[73] B. Peeters, H. Van Der Auweraer, P. Guillaume, J. Leuridan, The PolyMAX frequency-domain method: a new standard for modal parameter estimation?, Shock and Vibration 11 (2004) 395–409. doi:10.1155/2004/523692.
[74] J.-P. Noël, G. Kerschen, Nonlinear system identification in structural dynamics: 10 more years of progress, Mechanical Systems and Signal Processing 83 (2017) 2–35. doi:10.1016/j.ymssp.2016.07.020.
[75] K. J. Moore, M. Kurt, M. Eriten, D. M. McFarland, L. A. Bergman, A. F. Vakakis, Wavelet-bounded empirical mode decomposition for measured time series analysis, Mechanical Systems and Signal Processing 99 (2018) 14–29. doi:10.1016/j.ymssp.2017.06.005.
[76] M. Feldman, Nonparametric identification of asymmetric nonlinear vibration systems with the Hilbert transform, Journal of Sound and Vibration 331 (14) (2012) 3386–3396. doi:10.1016/j.jsv.2012.02.025.
[77] V. Ondra, I. A. Sever, C. W. Schwingshackl, A method for non-parametric identification of non-linear vibration systems with asymmetric restoring forces from a free decay response, Mechanical Systems and Signal Processing 114 (2019) 239–258. doi:10.1016/j.ymssp.2018.05.010.
[78] N. E. Huang, K. Hu, A. C. C. Yang, H.-C. Chang, D. Jia, W.-K. Liang, J. R. Yeh, C.-L. Kao, C.-H. Juan, C. K. Peng, J. H. Meijer, Y.-H. Wang, S. R. Long, Z. Wu, On Holo-Hilbert spectral analysis: A full informational spectral representation for nonlinear and non-stationary data, Philosophical Transactions of the Royal Society of London A: Mathematical, Physical and Engineering Sciences 374 (2065) (2016) 1–21. doi:10.1098/rsta.2015.0206.
[79] V. Ondra, I. A. Sever, C. W. Schwingshackl, Non-linear System Identification Using the Hilbert-Huang Transform and Complex Non-linear Modal Analysis, in: G. Kerschen (Ed.), Nonlinear Dynamics, Volume 1: Proceedings of the 35th IMAC, A Conference and Exposition on Structural Dynamics 2017, Springer International Publishing, 2017, pp. 77–86. doi:10.1007/978-3-319-54404-5_8.